JOURNAL OF GEOPHYSICAL RESEARCH, VOL. 95, NO. B5, PAGES 7007–7025, MAY 10, 1990

Frictional Behavior and Constitutive Modeling of Simulated Fault Gouge

CHRIS MARONE,[1] C. BARRY RALEIGH,[2] AND C. H. SCHOLZ

Lamont-Doherty Geological Observatory and Department of Geological Sciences, Columbia University, Palisades, New York

This paper presents an investigation of the frictional properties and stability of frictional sliding for simulated fault gouge. In these experiments we sheared gouge layers (quartz sand) under saturated drained conditions and at constant normal stress (50-190 MPa) between either rough steel surfaces or Westerly granite surfaces in a triaxial apparatus. Surface roughness (60 to 320 grit) and gouge layer thickness (0-4.0 mm) were varied in the experiments with granite samples. Porosity ϕ was monitored continuously during shear. Our measurements indicate that granular gouge exhibits strain hardening and net compaction for shear strains γ less than 0.5-1.0. For $\gamma > 0.5$-1.0, sliding occurs at approximately constant shear stress and net compaction from one load/unload cycle to the next ceases. Dilatancy occurs at 1/3 to 1/2 the shear stress required for sliding and $d^2\phi/d\gamma^2$ becomes negative at about the peak stress in a given loading cycle, indicating the onset of shear localization. Oblique shear bands appear in the layers at $\gamma = 1.3$-1.5. Experiments with an initial gouge layer exhibit velocity strengthening (the coefficient of friction increases with slip velocity), and initially bare granite surfaces exhibit velocity weakening. The magnitude of velocity strengthening varies inversely with normal stress and directly with gouge thickness and surface roughness. In the gouge experiments the dilatancy rate $d\phi/d\gamma$ also varies with slip rate. Using a simple energy balance to relate volume change and frictional resistance, we find quantitative agreement between the measured change in dilatancy rate and friction following changes in slip rate. This indicates that velocity strengthening within granular gouge is the result of dilatancy. The slip rate dependence of $d\phi/d\gamma$ increases with gouge thickness and surface roughness, in agreement with the friction data. Our data therefore suggest that slip within unconsolidated granular material, such as some natural fault gouges, is inherently stable. The results thus provide an explanation for (1) the tendency of gouge accumulation to stabilize slip in laboratory samples, and (2) the tendency for aseismic slip within shallow (< 3-5 km) unconsolidated fault gouge and within unconsolidated sediments such as shallow alluvium and accretionary prisms.

INTRODUCTION

Since the work of *Brace and Byerlee* [1966], laboratory friction experiments have been considered a good analog for the behavior of natural faults. Natural faults generally contain gouge, which is the product of wear along the slipping surfaces, and there is growing evidence that gouge plays an important role in controlling the stability of natural faults [e.g., *Scholz et al.*, 1969; *Marone and Scholz*, 1988] as well as spatial and temporal variations in aseismic creep [*Crook*, 1984; *Williams and Magistrale*, 1989]. Thus an understanding of earthquake mechanics requires understanding the frictional behavior of gouge and gouge-rock systems. To that end, a number of studies have considered the effect of gouge on rock friction [*Byerlee*, 1967; *Engelder et al.*, 1975; *Byerlee and Summers*, 1976; *Logan et al.*, 1979; *Dieterich*, 1981; *Shimamoto and Logan*, 1981; *Morrow et al.*, 1986; *Raleigh and Marone*, 1986; *Biegel et al.*, 1989; *Tullis et al.*, 1989]. These studies have shown (1) that the generation of gouge during slip of initially bare rock surfaces results in an increase in frictional resistance [e.g., *Byerlee*, 1967; *Scholz et al.*, 1972], (2) that gouge tends to stabilize slip, relative to slip between bare surfaces [e.g., *Byerlee and Summers*, 1976], and (3) that shear localization features develop within gouge and these features may influence the stability of sliding [e.g., *Engelder et al.*, 1975; *Byerlee et al.*, 1978; *Logan et al.*, 1979; *Tullis et al.*, 1989]. Despite progress in identifying the effects of gouge on rock friction the underlying micromechanics of these effects remain poorly understood. An understanding of these micromechanics is required to apply properly the results of laboratory friction experiments to natural faults.

Recently, attention has focused on modeling the constitutive behavior and stability of frictional sliding within laboratory samples, with the aim of improving our understanding of earthquake mechanics [*Dieterich*, 1979, 1981; *Ruina*, 1980, 1983; *Rice and Ruina*, 1983; *Tullis and Weeks*, 1986]. The rate and state variable constitutive laws proposed by Dieterich and Ruina provide a basis for predicting repetitive unstable sliding events, without the need for resetting of static friction following each event, such as required by displacement weakening models [e.g., *Stuart*, 1979]. For the rate and state variable constitutive laws, instability may occur if frictional resistance decreases with increasing slip rate (so called velocity weakening), depending on the stiffness of the loading system and the size of the velocity perturbation [e.g., *Gu et al.*, 1984]. However, sliding is inherently stable for velocity strengthening. Thus attention has focused on the conditions under which laboratory samples exhibit velocity weakening or velocity strengthening, with the goal of predicting whether natural faults will slip seismically or aseismically [*Dieterich*, 1979, 1981; *Ruina*, 1980; *Johnson*, 1981; *Dieterich and Conrad*, 1984; *Solberg and Byerlee*, 1984; *Weeks and Tullis*, 1985; *Lockner et al.*, 1986; *Morrow et al.*, 1986; *Tullis and Weeks*, 1986; *Shimamoto and Logan*, 1986; *Blanpied et al.*, 1987*a,b*; *Chester*, 1988; *Biegel et al.*, 1989; *Tullis et al.*, 1989; *Cox*, 1990]. While this issue is clearly of fundamental importance, the application of these results to natural faults requires understanding the physical

[1]Now at Department of Geology, University of Melbourne, Parkville, Victoria, Australia and Division of Geomechanics, CSIRO.

[2]Now at School of Ocean, Earth Science and Technology, University of Hawaii, Honolulu.

Paper number 89JB02803.
0148-0227/90/89JB-02803$05.00

mechanisms for rate and state dependent friction within rocks.

In this paper we describe friction experiments in which porosity measurements are used in addition to conventional stress-strain data to investigate strain accommodation mechanisms and constitutive behavior of gouge. We varied normal stress, gouge thickness, and surface roughness in order to study their effects on friction in gouge and gouge-rock systems. Previous studies have shown that surface roughness and gouge thickness have important effects on the stability of frictional sliding. However, these studies have not separated the properties of slip *within* gouge from slip at the gouge-rock interface (boundary slip), leaving some ambiguity as to the controlling mechanism. Therefore, in some of our experiments we used a steel sample with artificially high surface roughness in order to minimize boundary slip and effects associated with the gouge-rock interface. The effect of surface roughness, gouge thickness, and boundary slip were studied in a complementary suite of experiments using Westerly granite samples.

EXPERIMENTAL AND ANALYTICAL TECHNIQUE

Constitutive Modeling

We modeled frictional behavior over slip rate changes using the rate and state variable constitutive relations proposed by *Dieterich* [1979, 1981] and *Ruina* [1980, 1983]. These friction laws are based on laboratory observations of friction in rocks and are intended to describe the manner in which frictional resistance varies with slip velocity and slip history. The laws include state variables that describe the dependence of the present frictional resistance on the surface's slip history, for example, on its previous slip rate. Equation (1) is a form of the rate and state variable friction laws given by *Rice and Gu* [1983]:

$$\tau = \sigma[\,\mu_o + b_i\,\psi_i + a\,\ln(V/V_*)] \qquad (1)$$

where, τ is shear stress, σ is normal stress, μ_o is a constant, which may be thought of as the overall friction level, ψ_i are state variables, V is the sliding velocity at the slip surface, V_* is an arbitrary reference velocity, and a and b_i are constants (see Figure 1). The evolution of the state variables following a change in load point velocity is expressed as

$$d\psi_i/dt = -\,[(V/D_{ci})\,(\psi_i + \ln(V/V_*)] \qquad (2)$$

where t is time and D_{ci} is a characteristic distance over which friction decays following a step change in load point velocity (note that D_c is equivalent to L of, for example, *Rice and Gu* [1983] and *Tullis and Weeks* [1986].) Figure 1 illustrates the effect of a sudden increase in slip rate by a factor of e (=2.718) for a one state variable constitutive law. The parameter a represents the immediate (direct) increase in friction upon an increase in load point velocity, and b is the magnitude of the subsequent displacement dependent decay to a new steady state. This decay occurs exponentially with characteristic displacement D_c. After friction reaches a steady state at a given velocity, $d\psi_i/dt = 0$, and thus the state variable at steady state is given by $\psi_i^{ss} = -\ln(V/V_*)$. Substituting ψ_i^{ss} in equation (1) shows that

$$a-\Sigma b_i = \Delta\mu^{ss}/\Delta(\ln V) \qquad (3)$$

where $\Delta\mu^{ss}$ is the steady state change in friction. If $a-\Sigma b_i > 0$, as shown in Figure 1, frictional resistance increases with increasing slip velocity (velocity strengthening), whereas if $a-\Sigma b_i < 0$, friction decreases with increasing slip velocity (velocity weakening).

To model slip along a frictional surface, it is necessary to combine the elastic interaction of the loading system (the apparatus in an experiment, or the surrounding rock for a natural fault) with the surface's constitutive behavior. For small surfaces, such as in our experiments, the interaction is adequately described by a slider block loaded by a single spring [e.g., *Gu et al.*, 1984]. Equation (4) relates the stiffness of the spring (loading system) to shear resistance at the load point for a slider block loaded by a spring of stiffness K:

$$d\tau/dt = K\,(V_o - V) \qquad (4)$$

Here, τ is the shear stress applied at the load point, V_o is the load point velocity, and V is the velocity at the slip surface. To model frictional behavior, Equations 2 and 4 are solved as a system of simultaneous equations, yielding μ as a function of time or displacement from the step change in load point velocity. We set V_o equal to V_* and used equation (1) to relate variables in equations (2) and (4). Because equation(s) 2 is nonlinear, we obtained solutions numerically, using an order 4 Runge-Kutta method [e.g., *Conte and de Boor*, 1980].

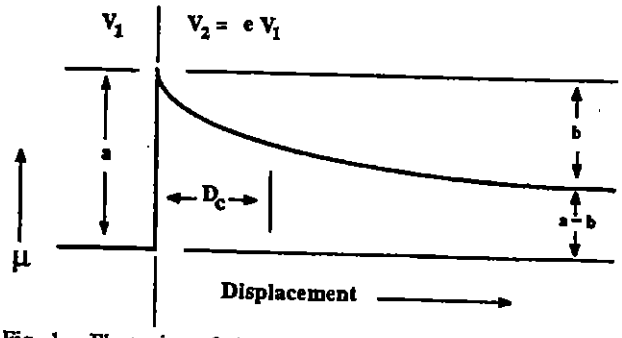

Fig. 1. Illustration of the slip rate and state dependent friction laws. A one state variable (ψ) law is shown for an idealized loading system of infinite stiffness. Upon an increase in slip rate from V_1 to $V_2 = eV_1$, the coefficient of friction μ increases by a (equation 1). With subsequent displacement, ψ (equation 2) decays according to $\psi = \psi_0\, e^{(-t/V_2/D_c)} + C$, resulting in a $1/e$ decay of μ over distance D_c (i.e., $\mu = \mu_0 + b[\psi_0\, e^{(-t/V_2/D_c)} + C] + a$, where $C = -\ln(V_2/V_*)$. The steady state slip rate dependence of μ is given by $a-b$ (equation 3). For a loading system of finite stiffness the direct increase in friction is less than a, and the parameters a, b, and D_c must be determined by modeling (e.g., Figure 12).

Experimental Method

We sheared water-saturated layers of Ottawa sand (>99% quartz) between surfaces cut at 45° to the axis of steel and granite cylinders. The layers were sheared under drained conditions (constant pore pressure, P_p, of 5 or 10 MPa) and at constant normal stress σ_n using a servocontrolled triaxial apparatus. Both steel and Westerly granite cylinders were used as the forcing blocks between which gouge layers were sandwiched, as shown in Figure 2. The steel sample was used to avoid complications in the porosity measurements such as microcracking and dilatancy adjacent to the shear zone. Ridges were machined into the steel surfaces perpendicular to the sliding direction to inhibit slip at the interface. These were 0.5 mm in height, triangular in cross section, and spaced every 0.75 mm. For the steel sample experiments, we used a single gouge thickness (4 mm) and effective normal stresses ($\sigma' = \sigma_n - P_p$) of 50-190 MPa. Above

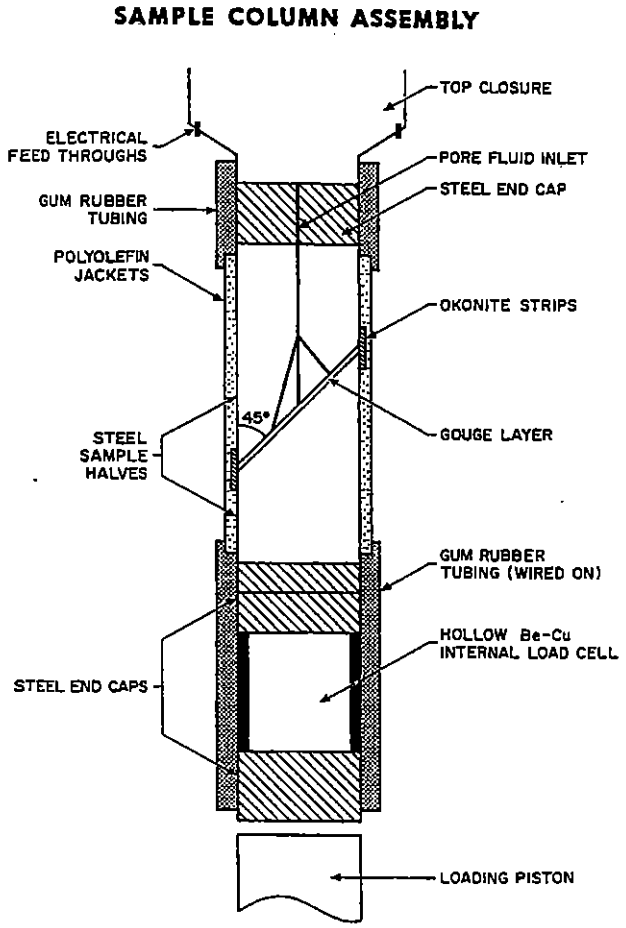

Fig. 2. Cross section of the sample column used for shear deformation of gouge layers at constant normal stress. Gouge layers were sheared within either steel or Westerly granite samples. Ridges of 0.5 mm height were machined on the steel surfaces and in a few cases on rock surfaces, perpendicular to the slip direction. An internal load cell was used to measure axial stress. Three pore fluid access holes provided fluid communication with the gouge layer. The diameter of the steel sample, end caps, and load cell is 3.5 cm. The sample length is 8.2 cm.

190 MPa, permeability of the gouge layers was insufficient to maintain drained conditions at slip rates above 0.5 μm/s. Westerly granite samples were used to study the effects of surface roughness and gouge thickness at 100 MPa σ'. We studied gouge thicknesses of 0 (initially bare surfaces) to 4 mm and surface roughnesses produced by polishing with 60, 120, and 320 grit. The ends of the granite samples were ground parallel (±0.0127 mm over the 8-10 cm length of the sample) and the 45° surfaces were ground to ±0.1°.

In preparing a gouge layer of given thickness, Ottawa sand was weighed dry (2.4 g per mm of thickness) to ensure reproducibility between experiments. In order to produce a uniform thickness, a polyolefin jacket was cut along a 45° angle and extended above the surface by a distance equal to the desired layer thickness. Two additional polyolefin jackets excluded the confining medium from the layer. Bicycle-tire inner tube (BIT) was used as jacketing in some of the experiments with Westerly granite, since, as discussed below, the polyolefin jackets have slip rate dependent strength. In the experiments with BIT jackets, a double layer of 0.05-mm-thick lead foil was used between the sample and inner-most jacket to inhibit jacket rupture with offset. For gouge layers thicker than 1 mm we found that BIT jackets flowed into the gouge, adversely effecting pore-volume measurements and frictional behavior, and thus these jackets were not used in experiments with >1-mm-thick layers.

Gouge layers were sheared by advancing the axial piston at a set displacement rate in servocontrol. Displacement along the sliding surface (δu) was measured with a linear variable differential transformer (LVDT) mounted external to the pressure vessel on the loading piston. In deriving shear displacement from axial displacement, we used the angle of the sliding surface and corrected for elastic shortening within the loading piston and sample column. The corrected value is used below. To avoid confusion, in the figures and text that follow the displacement rates given are axial displacement. We refer to the axial displacement rate as the load point velocity. We varied load point velocity between 0.010 and 30.0 μm/s. Shear strain γ was calculated as $\gamma = \delta u/w$, where w is the initial gouge thickness. Slip was limited to 13 mm to avoid sample misalignment.

All data were recorded digitally with a nominal sampling interval of 0.5 s. In the velocity stepping experiments described below, the sampling rate was increased/decreased by a factor of 10 upon a step increase/decrease in velocity so as to record an equal number of points per unit displacement. Shear stress and normal stress across the 45° surface were calculated from the axial load σ_1 and confining pressure P_c as: $\tau = (\sigma_1 - P_c)/2.0$; and $\sigma_n = (\sigma_1 + P_c)/2.0$

In order to observe porosity changes, independent of normal stress variations, normal stress across the gouge layer was maintained constant with servocontrol. This loading configuration results in slight changes in mean stress $(1/3[\sigma_1 + 2P_c])$; however, a few tests in which mean stress was held constant showed that this effect was negligible (this is to be expected since the layer thickness was always small relative to its other dimensions.) Constant normal stress was accomplished by using a signal from an internal load cell as the feedback to the confining-pressure servocontroller. Thus a change in axial load resulted in a simultaneous change in P_c in a 1:1 ratio so as to maintain a given normal stress across the 45° surface. The internal load cell was calibrated against an external load cell, using load differences to account for piston-seal friction. The confining pressure effect on the internal cell was electronically nulled using a scaled signal from a pressure transducer measuring P_c. Normal stress was constant to ±2% during shear loading and ±0.5% during slip rate changes, within the limit of the servocontrol response, which is 5-10 Hz. Changes in normal stress due to the reduction in sliding surface area with sample offset (about 25% per cm offset) were not accounted for by the servocontrol system; however, the data presented in this paper have been corrected for offset as described below. The normal stress values reported below are effective normal stress prior to offset.

Measuring pore volume change during triaxial shear. Pore volume changes were monitored during sliding by servocontrolling the pore pressure at a constant value (5 or 10 MPa) and measuring the fluid volume pumped into or out of the gouge. By measuring the displacement of a small-diameter piston a volume change of 10^{-5} cm^3 could be resolved. Three access holes (Figure 2) provided fluid communication with the gouge layer. For the experiments with granite samples the system was allowed to equilibrate

under pressure for several hours to ensure that the sample was saturated. We performed a series of tests to determine whether permeability was sufficient to maintain constant pore pressure within the gouge (see *Marone* [1989] for details), and found that pore pressure remained constant for displacement rates of ≤ 70 μm/s. We used displacement rates of ≤ 30 μm/s in our experiments.

The porosity of the gouge as it was packed along the sliding surface was 34 ±1%, as determined by weighing dry and saturated gouge layers. To estimate absolute porosity under load, we assumed 34% porosity at 0.5 MPa effective pressure (i.e., Pc = 10.5 MPa, Pp = 10 MPa) and measured pore volume change during hydrostatic loading. These measurements indicate that porosity was 18 ±1% at 100 MPa effective pressure prior to shear and 26, 22, 13, 12, and 11% at effective normal stresses of 50, 70, 150, 175, and 190 MPa, respectively. For comparison between experiments, we assume these porosities at γ=0 in the figures that follow.

Porosity corrections. Two effects may hinder pore volume measurements during triaxial shear. Each has to do with offset as the sample halves slide past one another. (1) A void may form at the position of the Okonite in Figure 2 if the jackets do not conform to the gouge layer with offset. Fluid filling such a void would be measured as volume increase. (2) The contact area between the sample halves decreases with offset. Thus normal stress increases within the central portion of the gouge layer while the ends of the layer experience unloading (from σ_n to P_c.) during offset. Each of these load changes causes a volume change. We have corrected the data presented here, using the change in contact area and the compressibility of the gouge layer (6×10^{-5}/MPa [*Marone* 1989]). For reference, the rate of porosity change with shear strain due to these combined effects is about 10% of the measured rate of porosity change during shear.

We tested for the possibility of a void forming with offset by running experiments with lead foil or Okonite, a soft self-vulcanizing rubber, between the sample and inner jacket (see Figure 2). These materials are soft enough to flow under even a slight differential stress and should therefore fill any voids. Pore volume measurements during experiments with and without these materials showed no differences, indicating that a void did not form with offset (see *Marone* [1989] for details).

Inherent resistance of the testing apparatus to frictional sliding. The slip rate dependence of friction in rocks is on the order of 1% per decade change in slip rate of their overall frictional resistance [e.g., *Dieterich*, 1979], and thus accurate measurements are difficult. Furthermore, although the inherent resistance to slip offered by a testing apparatus is generally a small fraction of a rock's overall friction level, it may be a large fraction of its frictional slip rate dependence. We undertook a series of tests to measure inherent resistance and its slip rate dependence in our triaxial setup. With reference to Figure 2 it is clear that two basic factors tend to inhibit slip along the 45° sliding surface: (1) stretching of the polyolefin jackets, and (2) sympathetic offset within the sample column (i.e., along horizontal surfaces) as slip occurs along the 45° surface.

We measured the stresses required for jacket stretching and sympathetic offset by sliding a steel sample with smooth 45° surfaces in the sample arrangement of Figure 2 [*Marone*, 1989]. Loctite anti-seize lubricant was used between end caps and on the sample ends, as in our experiments, and along the 45° surface. The steady state change in shear resistance, τ_{ss}, as measured on the 45° surface, per change in $\ln(V_o)$, where V_o is load point velocity, is given in Table 1 for polyolefin and BIT jackets and load point velocities of 0.1-30.0 μm/s. Slip velocity did not affect $d\tau_{ss}/d[\ln(V_o)]$ over the velocity range studied. We corrected our data by attributing the measured slip rate dependence of friction (Table 1) entirely to jacket effects and sympathetic offset. The correction is therefore a maximum estimate, since we assume no resistance (or slip rate dependence of the resistance) along the 45° surface. If the lubricated steel-on-steel 45° surface is itself velocity weakening/strengthening, we will underestimate/overestimate the inherent slip rate dependent resistance of the apparatus and experimental setup and thus overestimate/underestimate the actual slip rate dependence of gouge and rock friction. However, as the data (Table 1) show negligible normal stress dependence, but a strong dependence on jacket material, it is unlikely that slip along the 45° surface contributes significantly to slip rate dependent inherent resistance. The friction data presented below are corrected according to jacketing material and normal stress using the data given in Table 1.

TABLE 1. Inherent Resistance to Shear

Jacket Material	Number	σ', MPa	τ_o, MPa	$d\tau_{ss}/d[\ln(V_o)]$, MPa ±1 std
Polyolefin	3	100	0.55	0.06 ± 0.01
		50	0.37	0.04 ± 0.01
		30	0.12	0.04 ± 0.01
Polyolefin	1	100	0.28	0.03 ± 0.02
Bicycle tire inner tube	2	100	0.22	0.00 ± 0.005
		50	0.14	0.00 ± 0.005

Inherent machine resistance to shear for our triaxial apparatus and sample arrangement (see Figure 2). The increase in steady state shear resistance as a function of load point velocity ($d\tau_{ss}/d[\ln(V_o)]$) is given for different jacketing materials. The data do not show appreciable normal stress dependence, suggesting that end caps do not provide a significant slip-rate dependent resistance. τ_o is the resistance (±0.05) as measured at 1.0-mm offset. Jacketing materials were: Polyolefin, RNF-100 Shrink Tube, 1.5-inch O.D., 4:1 shrink ratio; and Bicycle Inner Tube, Cycle Products Company, York, Pennsylvania, part no. 983, 1.375-inch I.D., middleweight.

RESULTS

Evolution of Frictional Strength and Porosity

In the majority of our experiments we deformed gouge layers by repeatedly cycling the shear load from zero to failure. Load cycling was accomplished by advancing the axial piston, causing shear stress to rise, and retracting the piston after an arbitrarily-defined increment of shear strain γ (e.g., Figure 3). We also deformed gouge layers in a single shear load cycle. We begin by describing the results of multiple-cycle experiments.

Shear within rough steel surfaces. The overall behavior of the 85 experiments performed using the steel sample can be summarized as follows. During the initial load cycles the gouge underwent strain hardening and compaction (Figure 3). Note that each increase and decrease in normalized shear

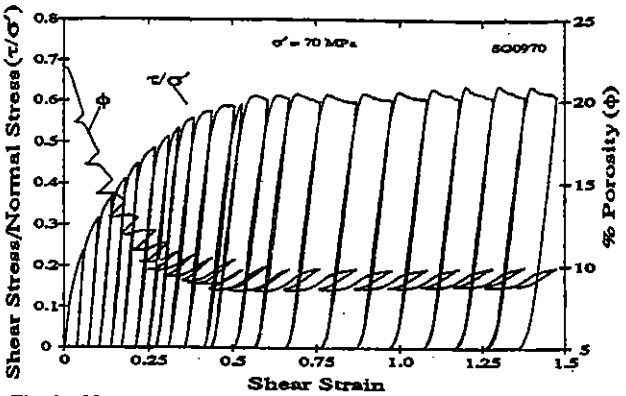

Fig. 3. Normalized shear stress τ/σ' and porosity versus shear strain for a 4.0-mm-thick gouge layer sheared within rough steel surfaces. Effective normal stress was constant during shear loading in all experiments. We refer to each increase and decrease in τ/σ' as a load cycle. Overall compaction occurred during the initial increments of strain, after which shear occurred at constant shear stress and porosity maintained a roughly constant level as measured at the end of each cycle.

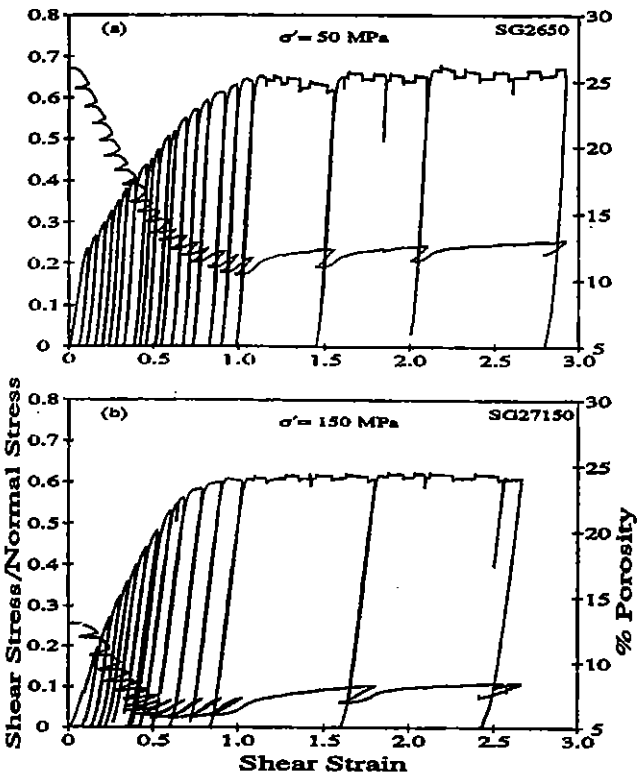

Fig. 4. Frictional and porosity behavior at two different normal stresses; 4.0-mm-thick gouge layer sheared within rough steel surfaces. Higher normal stress resulted in reduced porosity and a shorter period of net compaction. Small variations in porosity and shear stress during slip are due to changes in load point velocity. Figure 11 is an enlargement of the latter portion of Figure 4*b*.

stress (shear stress/effective normal stress = coefficient of friction during sliding) represents a "load cycle." For the first few cycles the stress-strain curves for unloading of one cycle and reloading of the next plot over one another ($\gamma <$ 0.25 in Figure 3), after which considerable hysteresis can be observed. During the initial increments of shear strain, compaction occurred upon both loading and unloading. With increasing strain, dilatancy occurred during loading, followed by compaction during sliding/yield. In general, for $\gamma <$ 0.5-1.0, load cycling resulted in strain hardening and net compaction. After a shear strain of 0.5-1.0, the stress-strain curve for each cycle exhibits a peak stress followed by a decrease and sliding at a roughly constant shear stress. In each experiment the appearance of these peaks in stress marked a transition from overall strain hardening to slip at an approximately constant shear stress (Figure 3). Net compaction also ceased at γ = 0.5-1.0, and additional shear occurred at roughly constant porosity, as measured at the end of each load cycle.

The effect of greater normal stress was to reduce porosity and shorten the stage of strain hardening and compaction (Figure 4). At 50-MPa effective normal stress, porosity reached a roughly constant level of 11-13% at γ = 0.9-1.1 (Figure 4*a*), whereas at 150-MPa σ', porosity was reduced to 5-7% by γ = 0.4-0.6 (Figure 4*b*). Comparison of Figures 3 and 4 indicates the experimental reproducibility in the overall mechanical behavior. At a given normal stress, scatter in the friction data was ± 2-3%. For the normal stress range studied, shear was accommodated without significant strain hardening for $\gamma >$ 0.5-1.0.

After a shear strain of 0.5-1.0, the net porosity change over a given load cycle depended on the amount of shear displacement in that cycle (Figure 5). Net dilatancy occurred in long-displacement cycles (those in which a peak stress occurred followed by inelastic displacement, i.e., from C to D in Figure 5*a*), and net compaction occurred in elastic cycles (those without appreciable inelastic displacement, i.e., just before B and C, from D to E, E to F, and F to G, Figure 5). Thus the net pore volume increase that occurred in long-displacement cycles was recovered upon subsequent elastic shear loading. In contrast, compaction did not occur when the layer was subjected to hydrostatic loading following net dilatancy (P_c was repeatedly cycled from 100 to 50 MPa following E, Figure 5). This indicates that net dilatancy during long-displacement cycles occurred within that portion of the gouge layer subjected to shear load (i.e., not within parts that have slid out of the contact area with offset) and not as an artifact of jacketing or gouge layer offset. In the latter case, hydrostatic load cycling should also cause compaction, since the offset portion of the gouge layer experiences the same pressure change during pure shear loading and hydrostatic loading. As discussed below, these observations indicate that net dilatancy in long-displacement cycles occurs as a result of unpacking of an overconsolidated gouge.

In single-cycle experiments, rapid strain hardening and compaction occurred for $\gamma <$ 0.5-1.0 (Figure 6). Dilatancy began at γ = 0.5-1.0 and continued throughout yield for the shear strains attained in our experiments ($\leq$ 3.3). Single-cycle experiments showed significantly less compaction than multiple-cycle experiments at a given effective normal stress; at 100 MPa, single-cycle experiments compacted to 12-14% porosity compared with 7-9% in multiple-cycle experiments at similar shear strains.

Porosity changes. Compaction was the sole porosity response to shear during the initial increments of shear strain in both single- and multiple-cycle experiments

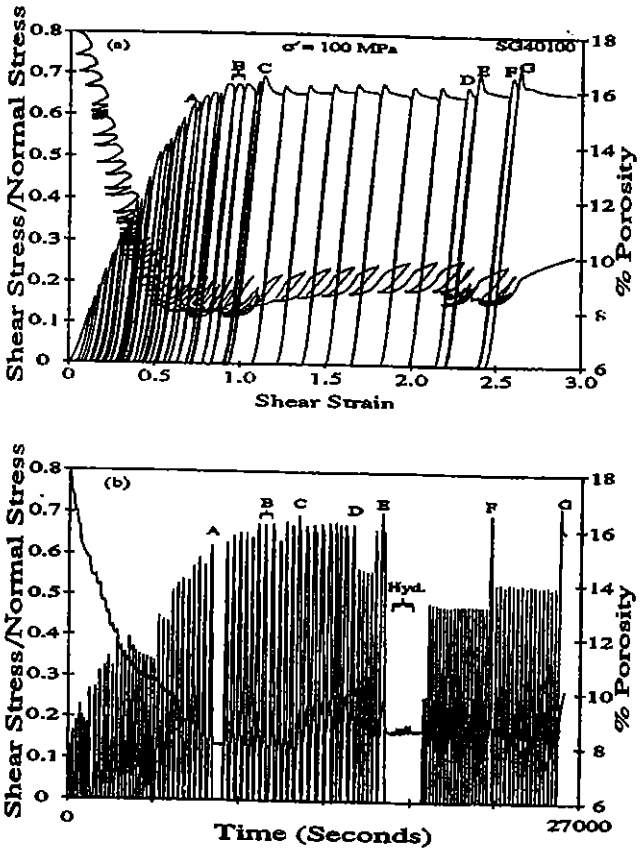

Fig. 5. Normalized shear stress and porosity versus (*a*) shear strain and (*b*) time for a 4.0-mm-thick gouge layer sheared within rough steel surfaces. The data in Figure 5*a* are plotted versus time in Figure 5b and a few key load cycles are marked in each plot to facilitate comparison. Note that because repeated elastic loading cycles overlay in Figure 5*a*, a comparison of Figures 5*a* and 5*b* is needed to understand the experiment. Net dilatancy occurred in long-displacement cycles (those in which a peak stress occurred followed by inelastic displacement, i.e., from C to D in Figure 5a), and net compaction occurred in elastic cycles (those with negligible inelastic slip, i.e., the cycles before B and C, those from D to E, E to F, and F to G). See text for further explanation.

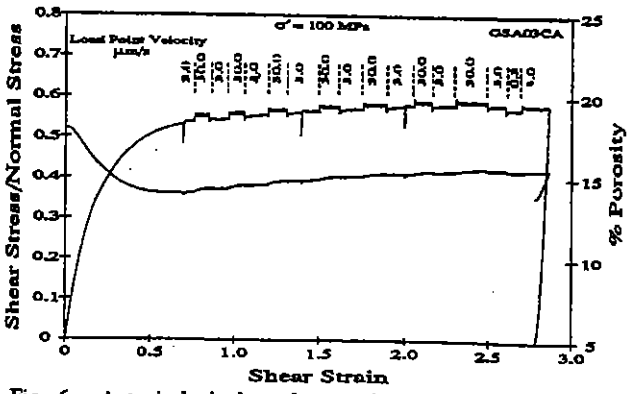

Fig. 6. A typical single-cycle experiment; 4.0-mm-thick gouge layer sheared within rough steel surfaces. Compaction and strain hardening occurred for $\gamma < 0.7$. Strain hardening continued at a slow rate for $\gamma > 0.7$ in single cycle experiments. Variations in normalized shear stress and porosity during sliding are due to changes in load point velocity as indicated directly above the τ/σ' curve. The three vertical segments of the shear stress (and porosity) curves represent brief periods of unloading.

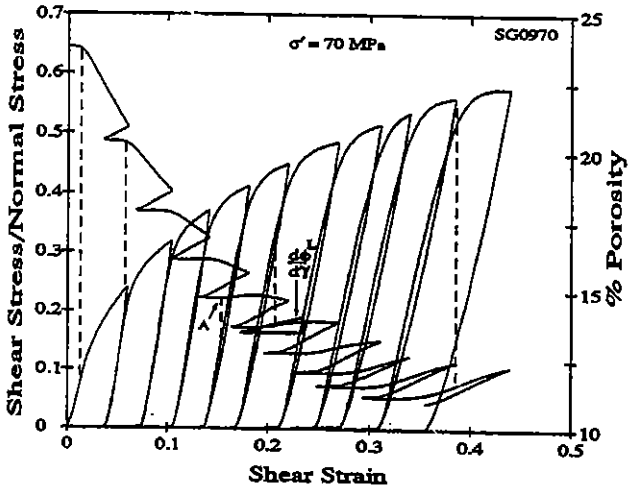

Fig. 7. An enlargement of the net compaction stage of Figure 3. Dashed lines indicate corresponding positions on the friction and porosity curves. In the first few cycles these lines show that an increase in compaction rate coincided with the yield stress, which occurred at the highest previous strain, i.e., the point of unloading for the previous cycle. Dilatancy occurred for the first time at A followed by compaction with continued shear. The dilatancy rate as measured during during loading, $d\phi/d\gamma$, increased in successive cycles, as did hysteresis.

(Figures 3-6). Multiple-cycle experiments show that for $\gamma < 0.1$-0.2 the rate of compaction with strain increased at about the yield stress or maximum previous shear strain (Figure 7) and that consecutive load cycles exhibited successively lower compaction rates during yield. By $\gamma = 0.1$-0.3, dilatancy occurred during loading (A in Figure 7), followed by compaction at the maximum previous shear strain. The dilatancy rate as measured during the roughly linear portion of the loading curve, $d\phi/d\gamma^L$, increased in successive cycles throughout the stage of net compaction (Figure 7).

Following the stage of net compaction, $d\phi/d\gamma^L$ was constant from cycle to cycle as were the overall form of the porosity strain curves (Figures 3 and 8). The onset of dilatancy occurred at about 25% of the peak stress, and $d\phi/d\gamma$ increased initially and decreased during sliding (Figure 8). We calculated $d^2\phi/d\gamma^2$ from the digital data, and found that $d^2\phi/d\gamma^2$ became negative just prior to the peak stress (dashed lines in Figure 8). As shown by *Frank* [1965] and discussed later, the transition from positive to negative $d^2\phi/d\gamma^2$ indicates a transition from pervasive to localized shear.

Shear within Westerly Granite surfaces. In general, the behavior of "granite sample" experiments (Figure 9) was similar to that described above for shear within steel samples. Strain hardening and net compaction occurred for $\gamma < 0.5$-1.0, after which porosity reached a roughly constant value (as measured at the end of each cycle) and the stress-strain curves exhibited a peak stress. In contrast to the behavior observed for load cycling experiments with rough steel surfaces, strain hardening occurred after the net compaction stage (just prior to A in Figure 9). Strain hardening generally ceased following an abrupt decrease in

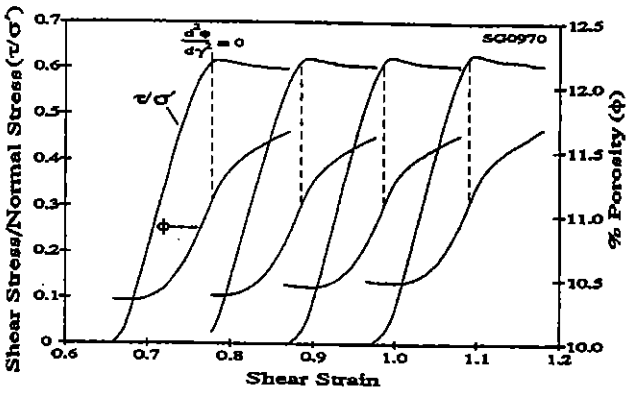

Fig. 8. An enlargement of the later stage of Figure 3. The curves have been truncated at the onset of unloading for clarity. Unlike the behavior at small strain (shown in Figure 7), neither $d\phi/d\gamma^L$ nor the form of the porosity-strain curves varied with progressive cycling. Dashed lines show the point at which $d^2\phi/d\gamma^2 = 0$.

frictional resistance (marked A in Figure 9), which was not an audible stick-slip stress drop but rather occurred over 5-10 μm of sliding. The drop in friction occurred after 4-7 mm of shear displacement, independent of gouge thickness or surface roughness for the ranges studied: 0.5-4 mm and 60 to 320 grit, respectively. To check the effect of surface roughness, we sheared 4.0-mm-thick layers within a granite sample with ridges machined into the surfaces the same as in the steel sample. These experiments did not show a drop in friction, and following the net compaction stage, slip occurred without strain hardening. The frictional and porosity behavior was the same as that for shear within the steel surfaces.

Microstructures

Thin sections of gouge layers subjected to shear within rough steel surfaces were examined for microstructures and particle-size distribution. In addition, we examined boundary slip for a suite of experiments with granite samples. The effects of shear strain and load cycling on particle-size distribution and microstructure are reported by *Marone and Scholz* [1989]. For the present purpose we focus on the microstructures and slip distribution within the layer. Figure 10 illustrates the prominent microstructures within the gouge layer and the location of boundary shears. The oblique structures are about 15° to the boundaries of the layer and thus are parallel to the R_1 (Riedel) shears described by *Logan et al.* [1979]. These features first appeared at shear strains of 1.3-1.5 in both single- and multiple-cycle experiments [*Marone and Scholz*, 1989].

Boundary slip along the gouge-steel or gouge-rock interface is indicated by the presence of streaks (left by darker grains) along the surfaces of the gouge layer. In the experiments with steel and grooved-granite surfaces, slip was limited to one half of each interface; this was always as shown in Figure 10. For the range of displacements studied (<13 mm), boundary slip did not occur over the entire length of either interface. Gouge layers deformed within granite samples roughened with 60, 120, and 320 grit showed slip along part of one boundary, as in Figure 10, and over the

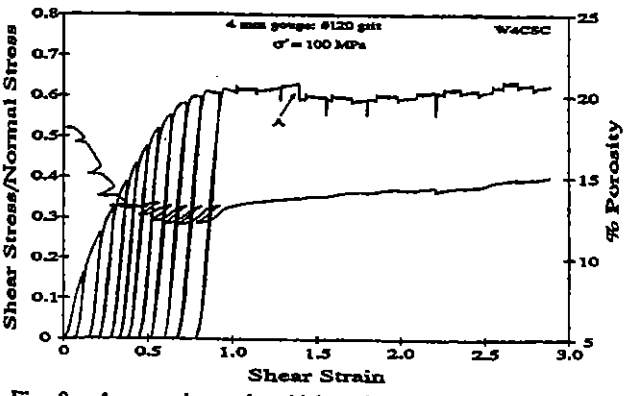

Fig. 9. An experiment in which a 4-mm-thick gouge layer was sheared within Westerly granite surfaces roughened with 120 grit (rms surface roughness of 1.3 μm ±0.2 as determined by profilometry). The normalized shear stress curve shows strain hardening prior to an abrupt drop in friction (A), after which slip occurs at a roughly constant stress level depending on slip rate. Vertical lines in the friction data represent short periods of unloading.

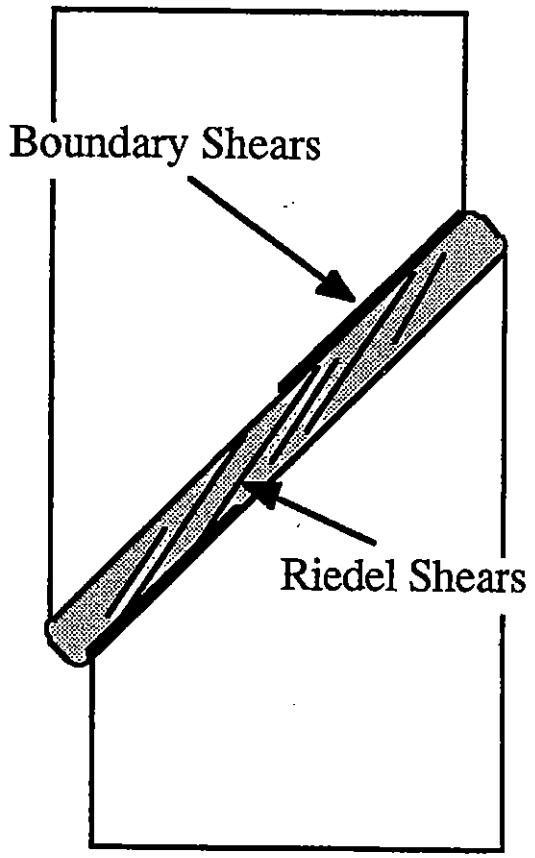

Fig. 10 An illustration showing the prominent microstructures within gouge layers and the location of boundary shears. The oblique structures are about 15° to the boundaries of the layer and thus are parallel to R_1 (Riedel) shears. Boundary shear was always limited to part of each interface (as shown) for layers sheared within grooved granite and rough steel surfaces. For shear within 60-320 grit granite surfaces, boundary shear extended along one entire interface and part of the other. We note that if boundary slip is limited to a portion of each interface, the observed slip distribution results in thinning of the layer with offset, whereas boundary slip that was limited to the opposite end of each interface would result in thickening of the layer with offset.

entire surface of the other boundary. Exceptions to this observation were layers sheared to less than about 3 mm, which showed boundary shear over only a portion of each surface as in Figure 10.

Slip Rate Dependence of Friction

Rough steel surfaces. In order to study the slip rate and state dependence of frictional resistance for the gouge and gouge-rock systems, we imposed sudden changes in load point velocity during sliding. In these "velocity-stepping experiments" the coefficient of friction was allowed to reach a steady value and a sudden (<1 s) change in load point velocity was imposed (Figure 11). Figure 11 was taken from the latter portion of Figure 4b, which indicates negligible overall variation in the friction level during velocity stepping. As indicated previously, porosity increased throughout long-displacement cycles after $\gamma = 0.5$-1.0 for the range of slip rates studied (0.1-30 μm/s). This produces the overall increase and concave-down shape of the porosity curve in Figure 11.

The general behavior shown in Figure 11 is typical of our experiments in which 4-mm-thick gouge layers were sheared within rough steel surfaces. A change in load point velocity resulted in an immediate (direct) change in μ and in dilatancy rate, both of the same sign as the velocity change, followed by a decay of opposite sign and smaller magnitude, a result termed velocity strengthening, since the steady state coefficient of friction increases with slip rate. The decay in friction following the direct effect occurred over about the same displacement for our range of slip rates and was thus displacement, and not time, dependent, in agreement with previous work [e.g., *Dieterich*, 1981]. The direct change in $d\phi/d\gamma$ following a velocity step decayed over about the same distance as the displacement dependent decay in friction.

To determine the overall effect of the change in load point velocity on dilatancy rate, we extrapolated the trend of the porosity curve prior to a given velocity step. The dashed lines in Figure 11 are extrapolations of best fit order 3 polynomials to several sections of the porosity curve prior to slip rate changes. Comparison of the dashed lines with the porosity data following a velocity step indicates that an increase in load point velocity caused an increase in $d\phi/d\gamma$ followed by a decrease of smaller magnitude, resulting in an overall increase in $d\phi/d\gamma$ (i.e., the curves diverge with increasing strain). Conversely, an overall decrease in $d\phi/d\gamma$ occurred for a decrease in load point velocity. Clearly, the long-term increase in $d\phi/d\gamma$ following an increase in slip rate is a transient phenomenon since porosity cannot increase indefinitely. However, the changes in $d\phi/d\gamma$ occur within the slip needed to reach a steady state friction level, and thus are relevant to the stability of sliding [e.g., *Rice and Ruina*, 1983]. The cause of dilatancy during sliding and the relationship between changes in friction and $d\phi/d\gamma$ are discussed below.

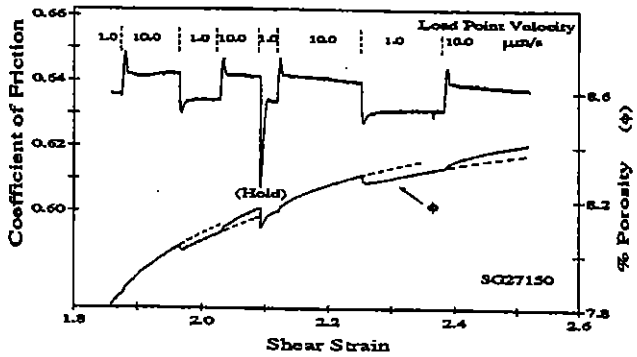

Fig. 11 An enlargement of the latter portion of Figure 4*b* showing several step changes in load point velocity for shear within rough steel surfaces. Displacement was stopped momentarily at the point marked "Hold." Step changes in load point velocity resulted in an immediate change in friction and in $d\phi/d\gamma$ of the same sign as the velocity step followed by a displacement dependent decay of opposite sign and smaller magnitude. Dashed lines show extrapolations of the porosity curve prior to a slip rate change. Comparison of porosity data over a velocity step with the extrapolation shows that $d\phi/d\gamma$ increased upon an increase in slip rate and decayed over the same distance as the decay in friction.

We modeled the frictional response to slip rate changes using rate and state variable constitutive laws [*Dieterich*, 1979, 1981; *Ruina*, 1980, 1983] described above, coupled with the elastic response of our apparatus. Our procedure was to measure $\Delta\mu^{ss}/\Delta(\ln V) = a - \Sigma b_i$ from the steady state portion of the friction data (see Figures 1 and 11) and to use this as a constraint while varying the parameters a, b_i, and D_{ci}. The stiffness K of our apparatus and sample is 0.105, 0.134, and 0.153 MPa/μm at effective normal stresses of 50, 100, and 150 MPa, respectively, as determined from load-displacement curves prior to slip.

We find that a one state variable model is sufficient to fit our data for 4.0-mm thick gouge layers sheared within the steel sample (Figure 12). The constitutive parameters are given along with each fit in Figure 12, and Table 2 gives the parameters for our suite of experiments. The value of a–b decreased with increasing normal stress but remained positive for the normal stress range studied. At a given normal stress, load point velocity reductions tended to show slightly higher values of a, b, and D_c than increases; however, a–b was not systematically different (Figure 12). The values of a–b were similar for single- and multiple-cycle experiments. For the range of shear displacements studied (< 13 mm), a–b did not vary systematically with total displacement after the stage of net compaction.

Figure 13 shows data from 110 measurements of a–b at effective normal stresses of 50 to 190 MPa. These data are corrected for apparatus and jacket effects (on the basis of the data given in Table 1) as indicated by the asterisk in Table 2. The mean value of a–b decreased from 0.0044 at 50 MPa to 0.0017 at 190 MPa (Figure 13). Constitutive modeling indicates that a–b decreases with normal stress as a result of a decrease in a and a slight increase in b with increasing normal stress (Figure 12 and Table 2). Thus, at 50 MPa σ' the direct increase in friction was larger and the displacement dependent decay that followed was smaller than at 150 MPa (Figure 12). D_c did not vary systematically with normal stress over the range studied (Table 2).

Westerly Granite surfaces. As in the steel sample experiments, we studied the slip rate and state dependence of friction in gouge sheared between Westerly granite surfaces. These experiments were intended to examine the effect of surface roughness and gouge thickness at a single effective normal stress (100 MPa). We studied surface roughnesses produced by 120 and 320 grit and gouge thicknesses from 0

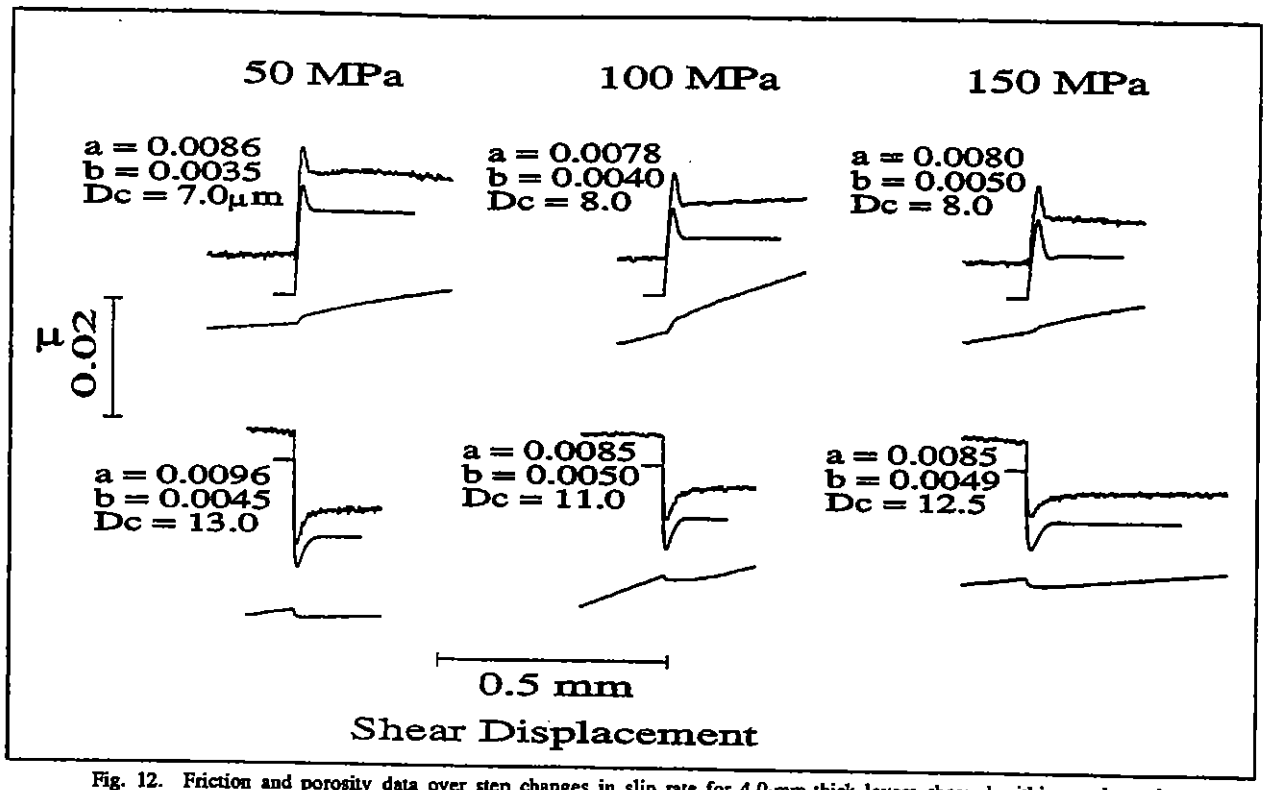

Fig. 12. Friction and porosity data over step changes in slip rate for 4.0-mm-thick layers sheared within rough steel surfaces. In each case, the friction data are plotted above a one state variable model fit, which has been offset downward for clarity, and porosity is plotted below. A 10x increase (top row) and decrease (bottom row) in load point velocity is shown for effective normal stresses of 50, 100, and 150 MPa; the simulations were done with a σ' value corrected for sample offset. Note that the direct change in friction and in $d\phi/d\gamma$ varies inversely with normal stress.

(initially bare surfaces) to 4 mm. We also ran velocity stepping experiments with 4-mm-thick gouge layers using a grooved-granite sample. We begin by describing the general behavior and stability of sliding for the different layer thicknesses and surface roughnesses and then present the constitutive parameters and porosity data.

As indicated in Figure 9, the general rate dependent behavior of the experiments with granite samples was similar to those using the steel sample. Velocity strengthening occurred for 4-mm-thick gouge layers, and slip was stable for all surface roughnesses and slip rate changes. For 1-mm-thick layers (Figure 14), stable sliding occurred for both 120 and 320 grit surfaces; however, for 320 grit surfaces slip became unstable following load point velocity increases of ≥ 5x. Small-amplitude stick-slip events persisted at ≥ 10 μm/s for the 320 grit surfaces, whereas at 5 μm/s, stable sliding occurred after a short period of unstable slip. Thus smoother surfaces and/or higher loading rates favor instability.

For 0.5-mm-thick layers sheared within 120 grit surfaces, unstable slip occurred for 10x increases in load point velocity from 2.0 to 20.0 μm/s (Figure 15), but sliding became stable after a period in which stick-slip events diminished in amplitude with displacement. As noted by *Rice and Gu* [1983] and *Tullis* [1988], this behavior is consistent with velocity strengthening and results from the elastic interaction between the slip surface and the loading system. In contrast, slip was stable for velocity steps from 0.2 to 2.0 μm/s. For 320 grit surfaces 0.5-mm-thick layers exhibited unstable slip at rates above 4-6 μm/s and for load point velocity increases > 3x. Due to the relatively large grain size of our starting gouge material (about 0.5 mm) we did not attempt to study gouge layers thinner than 0.5 mm. Experiments with no initial gouge layer (bare surfaces) showed unstable slip at all slip rates for 320 grit surfaces and stable slip, but velocity weakening, for 120 grit surfaces.

Table 2 gives the constitutive parameters for our suite of granite sample experiments. The experiments with an initial gouge layer exhibited velocity strengthening and were reasonably well fit with a one state variable constitutive model (Figure 16). Initially bare surfaces exhibited velocity weakening, and a two state variable model was necessary to fit the friction data (Figure 16). The magnitude of $a-b$ decreased with decreasing gouge thickness and surface roughness (Figure 17). The 4.0-mm-thick layers sheared within grooved surfaces (Figure 17) showed the largest values, which were about equal to those obtained for slip between rough steel surfaces. For 4.0-mm-thick layers, $a-b$ decreased from 0.0040 for shear between grooved granite surfaces to 0.0019 for 320 grit surfaces. For thinner layers, shear within rougher surfaces also resulted in greater velocity strengthening (Figure 17).

The dilatancy rate also changed upon a velocity step, and it decayed over about the same distance as the decay in friction (Figure 16). With decreasing gouge thickness, step changes in slip rate produced smaller changes in the dilatancy rate, $d\phi/d\gamma$, and smaller steady state changes in friction. Our

TABLE 2. Constitutive Parameters

Gouge Layer Thickness mm	σ' MPa	Velocity Range μm/s	a x10^{-3}	b x10^{-3}	D_c μm	$a-b$ x10^{-3}	$a-b^*$ x10^{-3}
			Steel Sample				
4.0	50	0.1-10.0	8.9 ± 0.8	3.7 ± 0.5	9.8 ± 2.0	5.2† ± 0.4	4.4
4.0	100	0.1-10.0	8.1 ± 0.3	4.5 ± 0.4	9.9 ± 1.7	3.6† ± 0.3	3.0
4.0	150	0.1-10.0	8.1 ± 0.3	5.0 ± 0.2	11.3 ± 4.0	3.1† ± 0.3	2.7
4.0	175	1.0-30.0	6.6 ± 1.0	4.2 ± 0.6	7.2 ± 2.3	2.4† ± 0.5	2.1
4.0	190	1.0-30.0	6.7 ± 0.6	4.7 ± 0.6	11.7 ± 3.2	2.0† ± 0.4	1.7
			Westerly Granite Sample				
4.0	100						
grooved		0.2-20.0	10.0 ± 0.9	5.4 ± 1.0	9.7 ± 0.5	4.6† ± 0.9	4.0
120 grit		0.2-20.0	11.7 ± 1.2	7.9 ± 1.2	3.8 ± 2.1	3.7† ± 0.8	3.1
320 grit		2.0-20.0	7.4 ± 1.7	4.7 ± 1.5	4.2 ± 2.3	2.7† ± 0.5	1.9
2.0	100						
320 grit‡		2.0-20.0	11.3 ± 1.7	10.1 ± 1.3	3.5 ± 0.7	1.3† ± 0.5	0.7
1.0	100						
120 grit		0.5-20.0	10.4 ± 1.4	8.8 ± 1.0	3.8 ± 2.3	1.6§ ± 0.7	1.6
320 grit‡		0.5-10.0	10.2 ± 1.3	8.0 ± 0.9	3.0 ± 2.5	1.0§ ± 0.7	1.0
0.5	100						
120 grit		0.2-30.0	14.3 ± 4.8	12.6 ± 4.6	2.2 ± 1.6	1.8# ± 0.7	1.5
320 grit‡		0.2-5.0	16.3 ± 2.5	15.3 ± 2.8	0.74 ± 0.25	1.0# ± 0.5	0.9

Initially Bare Surfaces

σ'	Velocity	a x10^{-3}	b_1x10^{-3}	b_2x10^{-3}	D_{c1}	D_{c2}	$a-\Sigma b$x10^{-3}	$a-\Sigma b^*$x10^{-3}
100	0.2-10.0	23.8	19.7	6.4	2.7	70.8	−1.8§	−1.8
120 grit		± 11.5	± 10.1	± 2.5	± 2.4	± 18.6	± 2.0	

Mean and standard deviation for rate and state variable constitutive parameters. The "steel sample" data represent 110 measurements from 45 experiments. The "Westerly granite sample" data represent 88 measurements from 21 experiments.

*Corrected for jacket effects (see Table 1).

†Samples jacketed with three polyolefin jackets.

‡Unstable slip generally occurred for velocity increases of ≥ 5x and for slip velocities at the high end of the indicated range.

§Samples jacketed with two bicycle inner tube jackets.

#Data from experiments with either polyolefin or bicycle inner tube jacketing.

system of measuring pore volume was not sufficiently accurate for use in the bare surface experiments.

The numerical simulations (Figure 16 and Table 2) indicate (1) that the decrease in $a-b$ with gouge thickness is mainly due to an increase in b with decreasing gouge thickness; (2) that D_c (compare D_{c1} for the two state variable model) was largest for shear within the steel and grooved granite surfaces; (3) that D_c was approximately independent of gouge thickness for cases in which boundary shear occurred (shear within 120 and 320 grit surfaces); and (4) that a second longer characteristic length D_{c2} became apparent in the bare surface experiments.

Comparison With Previous Work

Our results for initially bare granite surfaces agree with previous work [*Dieterich*, 1979; *Ruina*, 1980; *Tullis and Weeks*, 1986; *Blanpied et al.*, 1987*a*]. *Dieterich's* [1979] data are for slip at 6 MPa normal stress and show slightly stronger steady state velocity weakening ($a-b = -0.007$) compared with our bare surface experiments ($a-b = -0.002$ at 100 MPa). *Tullis and Weeks'* [1986] data were obtained at normal stresses of 27 to 84 MPa and their steady state values of $a-b$ (−0.003) agree quite well with our data as do *Blanpied et al.'s* [1987*a*] data (−0.001 to −0.002) for

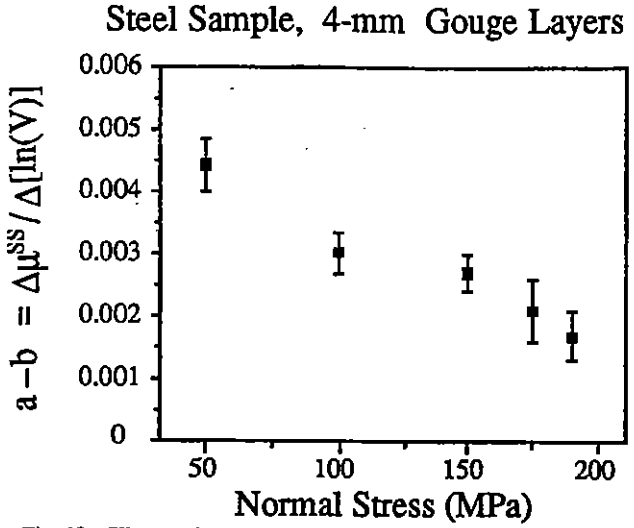

Fig. 13. Slip rate dependence of steady state friction ($a-b$* Table 2) as a function of normal stress for gouge sheared within rough steel surfaces. The mean value ±1 standard deviation is plotted for 110 measurements, roughly evenly distributed over the five normal stresses. The parameter $a-b$ varies inversely with normal stress as a result of decreasing a and slightly increasing b with increasing normal stress (see Table 2).

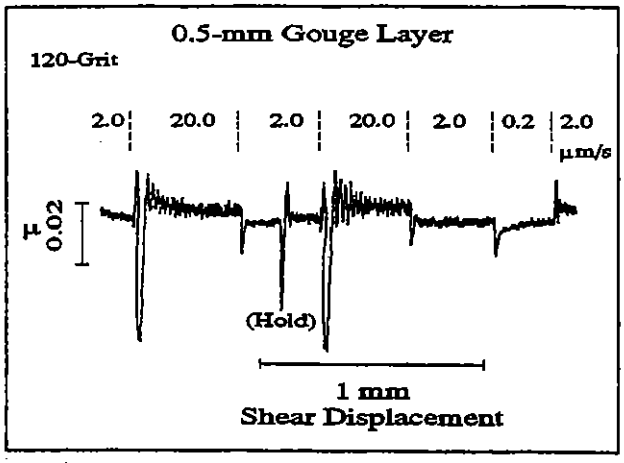

Fig. 15. Frictional behavior of a 0.5-mm-thick layer sheared within 120 grit surfaces. The coefficient of friction is plotted versus shear displacement and the load point velocity is given above the curve. Oscillatory stick-slip of decreasing amplitude occurred for velocity steps from 2.0 to 20.0 μm/s, whereas step velocity decreases and increases from 0.2 to 2.0 resulted in stable slip. Hold indicates a short period during which displacement was stopped.

comparable slip rates. This agreement is significant in that the data were obtained using different experimental configurations (*Dieterich* and Ruina's data in direct shear; Tullis and Weeks and Blanpied *et al.*'s data in rotary shear; and our data in triaxial shear), which suggests that the data represent the true behavior of rock on rock friction and not artifacts of experimental design.

Our results for shear of an initial gouge layer agree with data from triaxial experiments at 50–200 MPa σ' [*Solberg and Byerlee*, 1984; *Byerlee and Vaughan*, 1984; *Lockner et al.* 1986], and the small displacement portions of experiments at 10-25 MPa σ' by *Dieterich* [1981], *Biegel et al.* [1989], and *Tullis et al.* [1989]; note that *Tullis et al.* [1989] consider part of their earlier work to be invalid [*Blanpied et al.*, 1987*b*, 1988]. *Solberg and Byerlee* [1984] and *Byerlee and Vaughan* [1984] sheared 1-mm thick layers of crushed Westerly granite between 80 grit surfaces and found $a-b$ values of about 0.003 at 50-200 MPa. Their data indicate increasing $a-b$ with normal stress for the range 2.5-50 MPa; however, above 50 MPa their data show considerable scatter and are consistent with constant or decreasing $a-b$ with increasing normal stress. *Tullis et al.*'s [1989] data, for 1-mm gouge layers sheared within rough surfaces, show positive to neutral $a-b$ for displacements comparable to ours and velocity weakening to neutral $a-b$ for displacements from 20 to 100 mm.

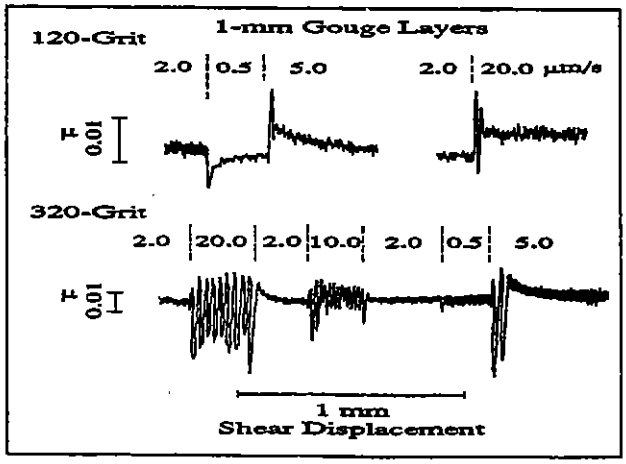

Fig. 14. Frictional behavior for 1-mm-thick layers sheared within 120 and 320 grit surfaces. The coefficient of friction is plotted versus displacement and the load point velocity (μm/s) is given above each curve. Unstable slip occurred upon velocity increases of ≥ 5x for layers sheared within the 320 grit surfaces. Stick slip persisted for slip rates ≥ 10 μm/s, whereas stable sliding occurred after a few stick-slip events at 5 μm/s.

Dieterich [1981] and *Biegel et al.* [1989] observe decreasing $a-b$ with displacement from 0 to about 4 mm, and a transition from velocity strengthening to velocity weakening at 4-5 mm for 1- and 3-mm-thick gouge layers sheared within 60 to 600 grit surfaces at 10 and 25 MPa σ'. In their experiments the period of decreasing $a-b$ coincides with strain-hardening, as in the net compaction and strain hardening stage of our experiments. This strain hardening makes measurements of slip rate dependent changes in friction difficult, so we did not measure $a-b$ during this stage but rather limited our measurement to the roughly steady state portion of the friction curve after net compaction. Since our total shear displacement is limited to 13 mm, thinner layers experience greater total shear strain, and we considered the possibility that $a-b$ varied with gouge thickness due to variations in shear strain. However, in a given experiment, $a-b$ did not vary with shear strain or displacement after the net compaction stage, which would be expected if differences in total strain caused the thickness dependency of $a-b$.

Dieterich [1981] attributed velocity strengthening for simulated gouge to "conditioning" associated with a

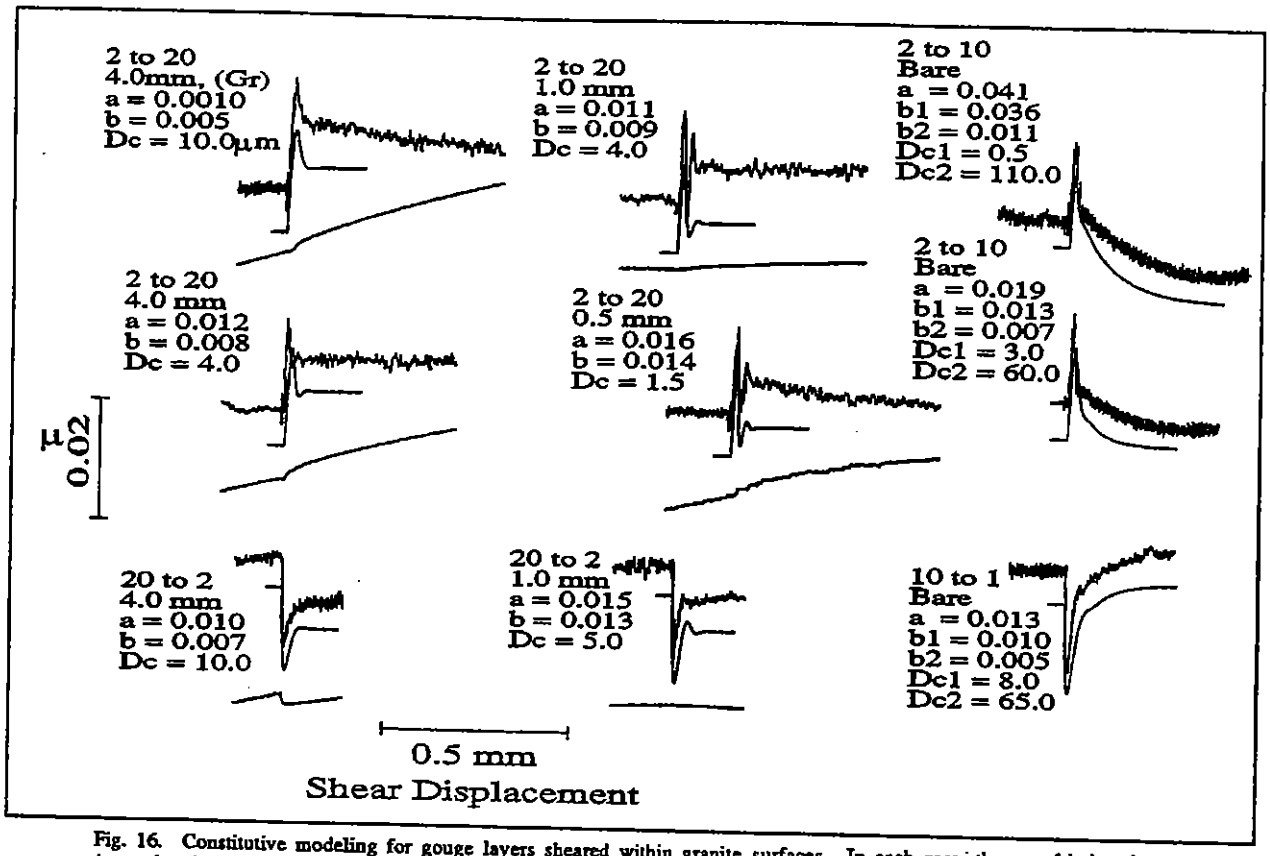

Fig. 16. Constitutive modeling for gouge layers sheared within granite surfaces. In each case, the raw friction data (note electrical noise) are plotted above a rate and state variable numerical simulation, which has been offset downward for clarity, and porosity is plotted below (except for the cases of initially bare surfaces.) The load point velocity (μm/s) before and after the velocity step is given first, followed by the gouge thickness and constitutive parameters. The data are for slip within 120 grit surfaces, except for that at the top left labeled (Gr), which is for shear within a grooved sample. Note that velocity strengthening occurs for shear of an initial gouge layer, whereas initially bare granite surfaces exhibit velocity weakening.

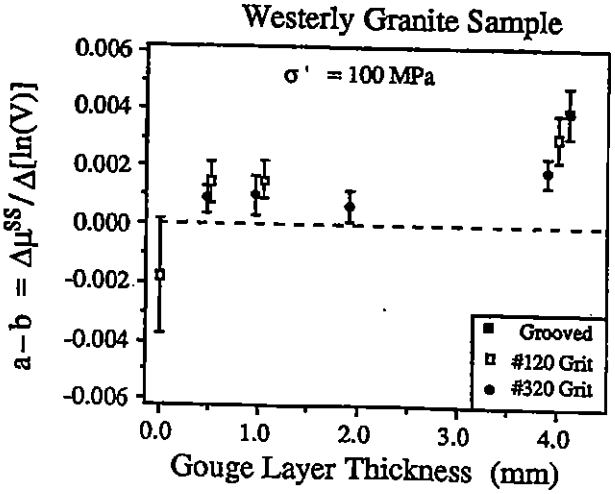

Fig. 17. Mean values of $a-b$ ±1 standard deviation are plotted as a function of gouge layer thickness and surface roughness (data from Table 2). Data for 320 grit and grooved surfaces are offset horizontally for clarity. The data are corrected for jacket and apparatus effects; $a-b$ decreased with decreasing gouge thickness and, at a given gouge thickness, was lower for smoother surfaces. Initially bare 320 grit surfaces exhibited dominantly unstable slip, and therefore we did not measure $a-b$ but would infer velocity weakening from the unstable nature of slip.

presumed high comminution rate within the initial increments of shear and indicated that velocity weakening was observed after the shear strength had stabilized. In our experiments, velocity strengthening occurred after the shear strength had stabilized. In addition, the comminution rate was greatest for $\gamma < 1.5$ [*Marone and Scholz*, 1989], after which the particle-size distribution was approximately constant with further shear. This particle-size distribution is equivalent to (1) that found in experiments by *Biegel et al.* [1989]; (2) that for a natural fault gouge [*Sammis et al.*, 1987]; and (3) the theoretical steady state value derived by *Sammis et al.* [1987]. Thus our observation of velocity strengthening and negligible displacement dependence of $a-b$ for $\gamma > 1.5$ is apparently not related to insufficient comminution. Nevertheless, *Tullis et al.* [1989] find a correlation between the onset of velocity weakening and the development of boundary parallel shears (Y shears), and thus the possibility exists that continued comminution and reduction of mean grain size results in decreased $a-b$.

Tullis and Weeks [1986] also report a displacement dependence of $a-b$ for initially bare granite surfaces. Their measurements indicate velocity weakening of decreasing magnitude with displacement over the range 0-20 mm. Although our experiments with initially bare granite surfaces do not show a displacement dependence for $a-b$ over the

range studied, our data agree with those of *Tullis and Weeks* [1986] for larger displacements. We note that *Tullis and Weeks'* [1986] observation of increasing $a-b$ with displacement is consistent with our observation of increasing $a-b$ with increasing gouge thickness, since as indicated by *Power et al.* [1988], a gouge layer accumulates in their experiments during the stage (0-20 mm), which coincides with increasing $a-b$.

INTERPRETATION OF RESULTS

Evolution of Frictional Behavior

Our experiments indicate a transition in mechanical and porosity behavior at $\gamma = 0.5$-1.0 (Figures 3-10). Strain hardening and net compaction occur for $\gamma < 0.5$-1.0, whereas for $\gamma > 0.5$-1.0 slip occurs at constant shear stress and porosity maintains a roughly constant value, as measured after each load cycle. A similar transition is observed in soil mechanics experiments [*Lambe and Whitman*, 1969]. Loose soils undergo strain hardening and compaction during yield, while dense soils exhibit a distinct peak stress followed by decay to a "residual strength." The transition from loose to dense behavior is attributed to dilatancy and, at higher stresses, particle fracture, which must occur to accommodate strain within densely packed material [*Lambe and Whitman*, 1969].

Our results are consistent with this interpretation. For $\gamma <$ 0.5-1.0, shear strength increases while porosity decreases. In multiple-cycle experiments, each load cycle begins at a lower porosity and shows a higher dilatancy rate during loading than previous cycles. For $\gamma >$ 0.5-1.0, net porosity reduction ceases and successive cycles exhibit similar stress-strain-porosity relationships. Stress-strain curves exhibit a peak stress during loading followed by a period of decay and slip at constant stress. The magnitude of the peak stress and the dilatancy rate during loading correlate with the state of compaction; i.e., a higher peak stress and $d\phi/d\gamma^L$ occur following elastic shear load cycling and compaction (Figure 5). Thus our data show (1) that shear strength increases with compaction and (2) that a roughly steady frictional resistance is reached as porosity reaches an approximately constant value, as measured at a given shear stress. The particle size analyses of *Marone and Scholz* [1989] show that single- and multiple-cycle experiments produce identical changes in particle-size distribution with shear strain. For both types of experiments the initial stage of compaction coincides with rapid changes in particle-size distribution. This means that the greater degree of compaction in multiple- as compared to single-cycle experiments is due to increased packing between grains, and not additional particle size reduction and comminution. Thus the frictional strength of gouge reaches a steady level at a critical particle-size distribution or strain.

Shear Localization and the Onset of Yield

Load-cycling experiments show progressively higher dilatancy rate, $d\phi/d\gamma^L$, in successive cycles for $\gamma <$0.5-1.0 (i.e., Figures 3 and 7). For $\gamma >$ 0.5-1.0, the dilatancy rate is constant from cycle to cycle, and $d^2\phi/d\gamma^2$ changes from positive to negative at about the peak stress in a given cycle (Figure 8). Each of these observations suggest a transition from homogeneous to localized shear at $\gamma =$ 0.5-1.0.

Frank [1965] showed that in a deforming aggregate, inhomogeneous deformation becomes possible at the transition from positive to negative $d^2\phi/d\gamma^2$. He argued that an aggregate will undergo homogeneous deformation when $d^2\phi/d\gamma^2 > 0$ because regions that have undergone relatively more deformation require relatively larger volume increase (and thus energy expenditure) for their next increment of strain. This can be understood if we write (equation 5) the total work expended during shear per unit volume of material, W, in terms of the work done against friction, W_f, and that due to volume change, $(\sigma' d\theta)$, where θ is volume strain [e.g., *Bishop*, 1954; *Edmond and Paterson*, 1972]:

$$W = W_f + (\sigma' d\theta) \tag{5}$$

For a thin layer such as in our experiments, volume increases, on average, against the effective normal stress across the layer, σ'. In addition, if the stress changes associated with volume change are small, $d\theta$ will be equal to $d\phi$, and we assume this equality. Equation (5) may be written in terms of shear stress, using the relation $W = \tau\, d\gamma$:

$$\tau = \tau_f + (\sigma' d\phi/d\gamma) \tag{6}$$

Equation (6) shows that the total shear resistance τ increases with $d\phi/d\gamma$. Thus, while $d^2\phi/d\gamma^2$ within an aggregate is positive, areas that have experienced lesser strain (and thus have lower $d\phi/d\gamma$) will accommodate yield first, resulting in pervasive strain. When $d^2\phi/d\gamma^2$ becomes negative, the situation reverses since the rate of volume increase in a given region becomes progressively smaller with increasing strain. This provides a positive feedback for shear localization because, within a given area, dilatant work against σ' decreases continually with strain.

Our data show the first distinct transitions from positive to negative $d^2\phi/d\gamma^2$ at $\gamma =$ 0.2-0.5. In a given load cycle after γ = 0.5, $d^2\phi/d\gamma^2$ becomes negative at about the peak stress (Figure 8). These data therefore suggest the onset of shear localization at $\gamma =$ 0.5-1.0 and that shear becomes relocalized at about the peak stress during subsequent loading, which is in good agreement with the observation of fully developed Riedel shears at $\gamma =$ 1.3-1.5 [*Marone and Scholz*, 1989].

Dilatant Nature of Shear

Aggregate materials undergo volume change as they are sheared [*Reynolds*, 1885], and thus it is not surprising that our experiments show dilatancy during shear loading, after an initial period of net compaction. However, it is generally assumed that dilatancy should cease once an aggregate passes through its peak strength during shear [e.g., *Lambe and Whitman*, 1969]. Why, therefore, do our experiments exhibit dilatancy ($d\phi/d\gamma > 0$) throughout slip for the range of displacements studied? Two possible explanations are (1) a void forms with offset at the position of the Okonite in Figure 2, and fluid filling this void is measured as dilatancy; or (2) the gouge layer becomes compacted below the porosity at which shear can occur at constant volume and dilatancy occurs as the material

decompacts. With regard to the first explanation, as indicated above, we performed a series of tests and found that a void did not form with offset. In addition, our data show that dilatant volume increase during long-displacement cycles occurs within the portion of the gouge layer subjected to shear stress and not at the ends of the layer (Figure 5). Thus we examine the hypothesis that dilatancy during inelastic shearing is associated with unpacking of an overconsolidated material.

Overconsolidation is used in soil mechanics to describe materials that are denser than the equilibrium porosity for a given state of stress [*Lambe and Whitman*, 1969]. The effect of overconsolidation is illustrated in Figure 18, which shows a stress-strain curve before and after a normal stress reduction from 70 to 30 MPa. The exaggerated peak stress in the first load cycle after unloading is due to a memory of the higher normal stress (overconsolidation). Although the gouge has an elastic response to the normal stress reduction, it retains a memory of its past state, which decays with shear displacement. The peak stress and form of the stress-strain curves in our multiple-cycle experiments are identical to those of overconsolidated soils. *Roscoe et al.* [1958] also showed that overconsolidation can occur during monotonic shear. For a wide range of initial densities, aggregates compacted prior to dilating during shear. Aggregates with high initial densities dilated over a longer displacement. Thus porosity changes in our single-cycle experiments are consistent with overconsolidation during the initial stage of compaction. To test the effect of normal stress, we ran a few experiments at 20 MPa σ'. These experiments showed compaction throughout shear, suggesting that comminution and grain size reduction at higher normal stress cause overconsolidation during the initial increments of shear.

As mentioned above, our data indicate that shear is localized during sliding for $\gamma > 0.5$-1.0. This would tend to restrict unpacking to a localized zone, thereby decreasing the dilatancy rate and extending the displacement over which dilatancy occurs. Since an individual oblique shear band can only accommodate a limited displacement, due to geometrical incompatibility at the boundary, dilatancy may occur during slip as oblique shear bands die out and new features form within dense overconsolidated areas. Clearly, dilatancy cannot occur indefinitely, and indeed our experiments show continually decreasing dilatancy rate during shear.

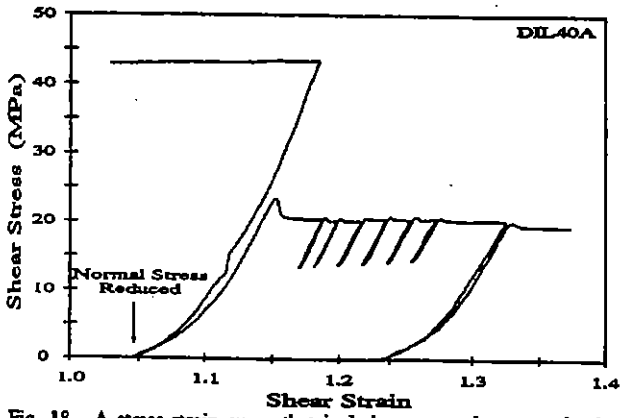

Fig. 18. A stress-strain curve that includes a normal stress reduction from 70 to 30 MPa; 4.0-mm-thick gouge layer. The exaggerated peak stress in the first load cycle after unloading is due to a memory of the higher normal stress (overconsolidation), which decays with shear displacement.

Constitutive Behavior

The observed slip rate and state dependence of friction can be fit by empirical rate-and state-variable friction laws (Figures 12 and 16). This modeling shows the following: (1) Slip *within* gouge (i.e., when boundary slip is minimized) results in velocity strengthening of decreasing magnitude with normal stress (steel and grooved Westerly granite samples). (2) The characteristic distance over which friction decays following a velocity step D_c is roughly constant over the normal stress range studied. This suggests that D_c does not vary with gouge particle size, which is expected to decrease with normal stress [*Engelder*, 1974; *Marone and Scholz*, 1989]. (3) When boundary shear occurs (smoother Westerly granite samples and thinner gouge layers), $a-b$ decreases relative to that for slip within gouge (Figure 17). This indicates that slip within gouge promotes velocity strengthening. In addition, D_c is largest when boundary shear is inhibited, and it does not change significantly with gouge thickness, suggesting that the entire width of the layer is not involved in shear. (4) The magnitude of $a-b$ decreases with decreasing gouge thickness as a result of a decrease in b.

Thin gouge layers sheared within smooth surfaces show persistent unstable sliding at high slip velocities. Although the magnitude of $a-b$ cannot be obtained directly for unstable slip, velocity weakening is implied [e.g., *Gu et al.*, 1984]. That is, sustained unstable sliding can occur only if the loading stiffness K is less than a critical stiffness K_{cr}; $K_{cr} = -(a-b)\,\sigma/D_c$. Positive values of $a-b$ result in stable sliding, with the possibility of unstable events for sufficiently large velocity jumps. For $K \approx K_{cr}$ (negative or very small values of $a-b$), oscillatory motion is possible, which decays to stable sliding for K slightly larger than K_{cr} and becomes periodic stick slip for K slightly smaller than K_{cr} [*Gu et al.*, 1984; *Tullis*, 1988; *Hobbs*, 1988]. Our 1-mm gouge layers show sustained unstable sliding when sheared within smooth (320 grit) surfaces at slip rates of ≥ 10 μm/s (Figure 15) and thus indicate $a-b$ of about 0 or slightly negative. Whereas for lower slip rates or rougher surfaces, stable slip and velocity strengthening are observed. The 0.5-mm-thick layers exhibit oscillatory motion that decays to stable sliding for 10x increases in velocity to 20 μm/s (Figure 15), suggesting $K \approx K_{cr}$ or $a-b$ of about 0 or slightly positive.

Relationship Between Dilatancy Rate and Friction of Gouge

Our velocity stepping experiments show a close correlation between changes in friction and porosity. In particular, the initial friction response to a velocity step and the subsequent decay occur over the same distance as changes in $d\phi/d\gamma$ (i.e., Figures 11, 12, and 16). The change in $d\phi/d\gamma$ requires a change in shear resistance as a result of energy expended in effecting a volume change against external stresses [equations (5) and (6)]. Thus the observed slip rate and state dependence of friction within gouge may be the result of changes in $d\phi/d\gamma$. We may evaluate the relationship

between friction and dilatancy rate as follows. Dividing equation (6) by σ' yields a relationship between the total coefficient of friction μ (this is the quantity measured in our experiments), the intrinsic coefficient of friction μ_f, and the frictional resistance associated with volume change ($d\phi/d\gamma$);

$$\mu = \mu_f + (d\phi/d\gamma) \quad (7)$$

The intrinsic coefficient of friction is that due to, for example, slip between particles, whereas μ is simply the shear resistance of the gouge layer divided by the effective normal stress. Equation (7) indicates that total frictional resistance is a function of the rate of volume strain with shear strain.

Because we measured porosity as a function of shear strain, we can quantitatively determine the contribution of $d\phi/d\gamma$ to μ during velocity stepping experiments. As a starting model we assume no change in μ_f with slip rate and consider the data from 4.0-mm gouge layers sheared within steel samples. For μ_f independent of slip rate, equation (7) predicts that a change in dilatancy rate results in a change in μ of magnitude $|d\phi/d\gamma|$. We determined the effect of a velocity step on $d\phi/d\gamma$ after removing the overall porosity trend prior to the velocity step (Figure 19*a*). We then calculated the change in friction due to the change in dilatancy rate (equation 7). The calculated and measured friction curves have identical form (Figures 19*b* and 20), and thus D_c is predicted quite well solely on the basis of the change in dilatancy rate. However, the change in friction calculated from $d\phi/d\gamma$ overpredicts both the direct and steady state change in friction. The amount by which the steady state change in friction is overpredicted ($\Delta\mu'$) increases with the size of the velocity step, but $\Delta\mu'/\ln(V_1/V_0)$ is approximately constant (Figure 21). That is, the difference between the measured increase in friction with slip rate and the increase caused by $d\phi/d\gamma$ scales with the logarithm of the velocity step. Thus the assumption that μ_f is independent of slip rate may be invalid. Indeed, we know that μ_f varies with slip velocity for bare rock surfaces. If we include a velocity weakening term in μ_f, which is equivalent to that measured in bare rock experiments ($a-b = -0.002 \pm 0.001$,) equation

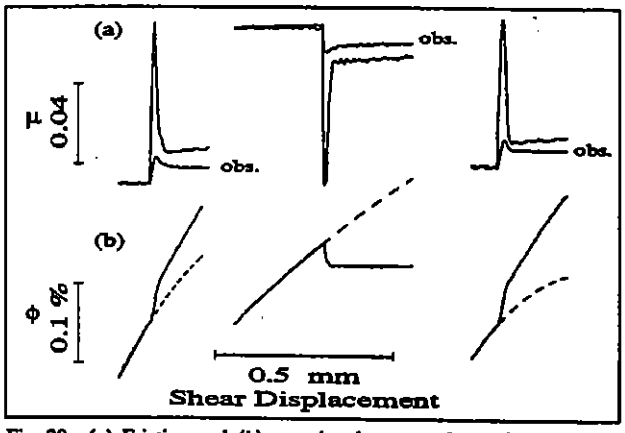

Fig. 20. (*a*) Friction and (*b*) porosity data over three 10x slip rate changes for 4.0-mm gouge layers sheared between rough steel surfaces at 100 MPa σ'. Dashed line represents the porosity trend prior to the slip rate change. The change in friction calculated on the basis of the change in dilatancy rate (equation 7) is plotted together with the observed change in friction (curves marked obs.). Both the direct and steady state change in friction are smaller than the calculated change assuming no change in μ_f with slip rate.

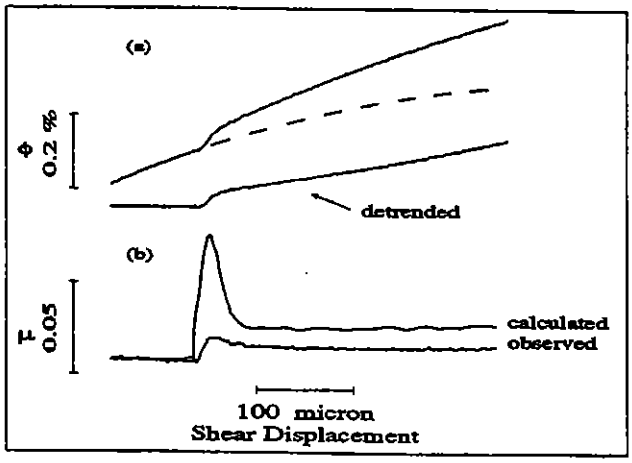

Fig. 19. Friction and porosity data over a 10x slip rate increase for a 4.0-mm gouge layer sheared between rough steel surfaces. (*a*) Upper curve shows measured porosity data. The dashed line is an extrapolation of the trend prior to the velocity step, and the difference between the two curves gives the effect of the velocity step on porosity (detrended curve). (*b*) Change in friction calculated on the basis of the change in $d\phi/d\gamma$ using equation (7) and the detrended ϕ curve. Note that the form of the two curves are identical and that the change in μ calculated from $d\phi/d\gamma$ overpredicts the measured change in friction.

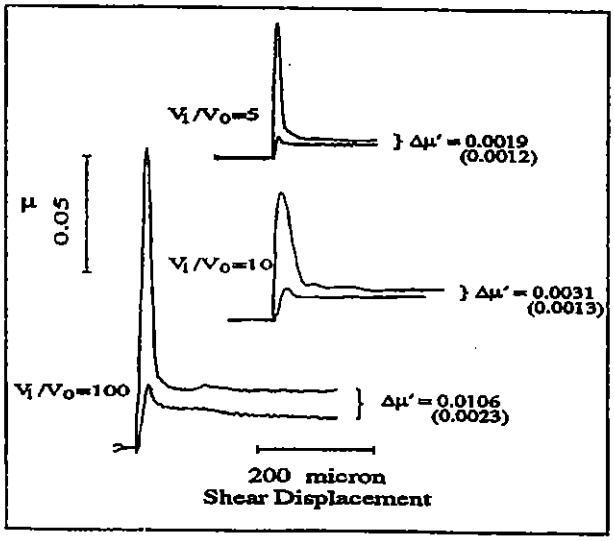

Fig. 21. The change in friction calculated on the basis of the change in dilatancy rate (equation 7) and the measured friction data (lower curve for each set) are plotted for different size velocity steps. The ratio of the final to initial slip rate is given along with the difference between the calculated and measured change in friction at steady state. The number in parentheses is the difference between the curves at steady state ($\Delta\mu'$) divided by $\ln(V_1/V_0)$: $\Delta\mu/\Delta[\ln(V)]$. The calculated change in friction overpredicts the measured change by a larger amount for larger slip rate changes but the difference scaled by $\ln(V_1/V_0)$ is approximately constant, suggesting that μ_f decreases with the log of the slip rate.

(7) predicts the measured steady state change in friction (Figure 21). This indicates that velocity strengthening in the gouge layers is the result of an increase in dilatancy rate with slip rate.

The relationship between μ and $d\phi/d\gamma$ given by equation (7) holds over the normal stress range studied (50-190 MPa) for 4.0-mm-thick gouge layers sheared between rough steel surfaces. However, even if the velocity weakening term is applied immediately upon the increase in load point velocity, the direct friction effect is overpredicted by the change in $d\phi/d\gamma$ (Figure 21). From equations (6) and (7) we see that a smaller change in friction occurs if volume increases against a stress less than σ'. That is, following a number of others [*Bishop*, 1954; *Lambe and Whitman*, 1969; *Mandl et al.*, 1977], we have assumed that volume increase occurs perpendicular to the long-term slip. Since the long-term slip direction must be parallel to the boundaries of the gouge layer, overall volume increase must occur against σ'. However, transient slip may occur at an angle to the layer, such as along Riedel shears. For transient slip along a Riedel shear, volume increase would be perpendicular to that surface and hence against a stress less than σ' (see Figure 10). For a Riedel shear at 15° to the gouge layer (30° to σ_1), volume increase would occur against an effective normal stress of $0.65\,\sigma'$ for $\mu = 0.6$. (Recall that in order to maintain constant normal stress, P_c is reduced as σ_1, and shear stress, increase; thus the stress across a given surface at other than 45° to σ_1 depends upon the coefficient of friction.)

We may calculate the change in friction following a velocity step under the assumption that transient slip occurs at 15° to the plane of the gouge layer and gradually becomes parallel to the layer over the distance required to reach a new steady state friction level (Figure 22). As above (Figure 21) a velocity weakening term for μ_f is applied immediately upon the increase in load point velocity. Although the steady state increase in friction is predicted quite well, the direct effect is still overpredicted. If the velocity weakening term for μ_f is applied after a displacement D_c or greater, the initial peak calculated from $d\phi/d\gamma$ is larger by about 40%. The uncertainty in the calculation of this peak value is only ±10%, and thus it does not seem as though transient slip along the Riedel shears can fully explain the direct effect. This may indicate that initial slip upon a velocity step occurs at a higher angle than 15° to the boundary (≈35° is required to fit the data in Figure 22.)

Quantitative agreement between the observed steady state change in μ and that predicted from $d\phi/d\gamma$ plus velocity weakening for μ_f holds over the range of slip velocities and normal stresses used in the steel sample experiments. This implies that the decrease in $a-b$ with increasing normal stress (Figure 13) is caused by a reduction in the slip rate dependence of $d\phi/d\gamma$, as can been seen qualitatively by comparison of the data shown in Figure 12. There is a larger increase in $d\phi/d\gamma$ upon a velocity step at lower normal stress. We performed a similar analysis for experiments in which gouge was sheared within granite surfaces (Figure 23). The data show that the steady state change in $d\phi/d\gamma$ with slip rate decreases with decreasing gouge thickness, in agreement with lower $a-b$ for thinner layers. These data therefore suggest that: (1) changes in $d\phi/d\gamma$ with slip rate cause velocity strengthening within gouge, due to the work involved in effecting a volume change, (2) velocity strengthening is reduced for smoother surfaces and thinner gouge layers because the change in $d\phi/d\gamma$ is proportionally smaller than for slip within rougher surfaces or thicker gouge layers, and (3) μ_f decreases with the logarithm of slip velocity, in agreement with previous work [e.g., *Dieterich*, 1979; *Tullis and Weeks*, 1986].

One possible explanation for the relationship between dilatancy rate and friction of gouge is that the dilatancy rate is a measure of the shear band width. This hypothesis has been proposed in Soil Mechanics (*Healy*, 1963; *Muhlhaus and Vardoulakis*, 1987), and we may make the following qualitative argument. Under this scenario, only material

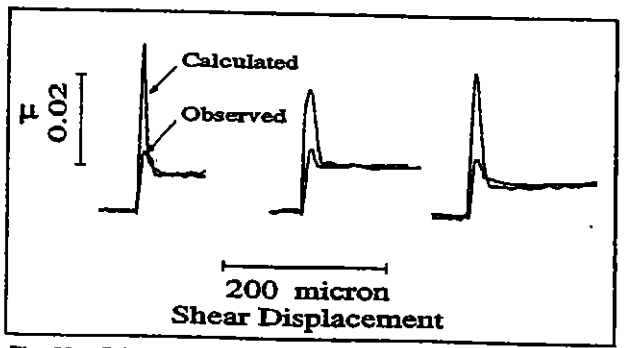

Fig. 22. Calculated and observed friction over three velocity steps assuming (1) an intrinsic steady state velocity weakening term of -0.002 $(a-b)$ for μ_f and (2) that transient slip occurs at 15° to the gouge layer. The calculated curve was derived using equation (7) with normal stress increasing linearly from $(0.65\,\sigma')$ to σ' over the (observed) slip distance required to reach a new steady state friction level. Note that the steady state change in friction is predicted quite well on the basis of the change in $d\phi/d\gamma$ and in μ_f and that the immediate increase in friction is overpredicted by a smaller amount than in Figures 19-21.

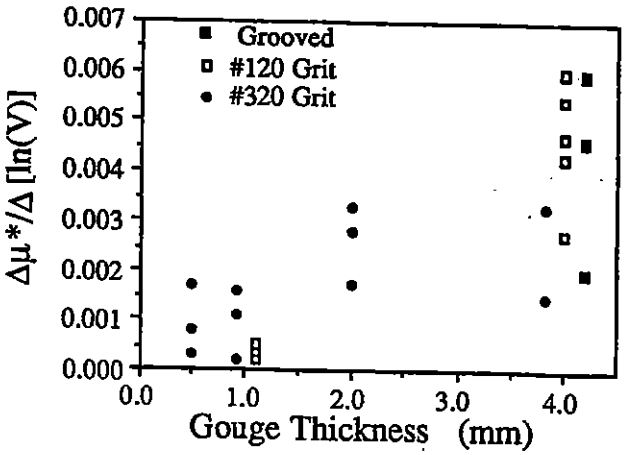

Fig. 23. The steady state change in friction with slip rate ($\Delta\mu^*$) predicted from the change in $d\phi/d\gamma$ (using equation 7) is plotted versus gouge thickness for layers sheared within granite surfaces. These data are for step increases in slip rate. The data indicate $\Delta\mu^*/\Delta\ln(V)$ varies inversely with gouge thickness, in agreement with the observation of lower $a-b$ for thinner gouge layers. Note by comparison with Figure 17 that $\Delta\mu^*/\Delta\ln(V)$ overpredict $a-b$ by about 0.002 ±0.001, in agreement with velocity weakening for the intrinsic coefficient of friction μ_f (see text for further explanation).

within a narrow band is actively involved in shear at a given slip rate, and the width of this band increases with slip rate. The mechanism for increasing shear band width can be understood if we assume that shear within gouge is accommodated by a combination of interparticle slip and rotation/fracture. Lower slip rates should favor interparticle slip since time dependent processes (such as stress corrosion cracking) will act to reduce stress inhomogeneity arising from geometrical incompatibility at slipping grain boundaries. In the simplest case, interparticle slip may involve only neighboring particles and those within a few grain diameters of the slip surface. This would produce thin shear bands and favor constant volume deformation. At higher slip rates, time dependent processes and interparticle slip cannot adequately accommodate shear and thus rotation/fracture will occur. Slip via rotation/fracture will involve particles several grain diameters from the slip surface, thereby increasing the shear band width and resulting in a slip rate dependence of dilatancy.

Our data are consistent with this interpretation. Several lines of evidence indicate localized shear within the gouge layers. Further, an increase in slip rate causes a transient and steady state increase in $d\phi/d\gamma$, which may be associated with increasing the shear band width. Under this scenario, a new equilibrium shear band width is attained after a small displacement. In our experiments, thinner gouge layers show lower values of $a-b$ and $d\phi/d\gamma$, which is predicted quantitatively by equation (7). The observation of a larger steady state increase in $d\phi/d\gamma$ and μ for thick layers, compared with thin layers, may indicate a larger increase in shear band width for thicker layers. Shear band width is thought to vary with mean grain size [*Muhlhaus and Vardoulakis*, 1987], and thus one possible explanation for the larger increase in width for thicker layers is a larger mean grain size in thicker layers. Alternatively, one may suppose that for sufficiently thin gouge layers the entire layer is involved in shear at a given slip rate and thus an increase in slip rate cannot cause an increase in shear band width. Under this assumption, there should be no increase in dilatancy rate for sufficiently thin layers and high slip velocities. This is consistent with our observation of unstable slip for higher slip rates at a given gouge thickness (Figures 14 and 15), since the observed change in $d\phi/d\gamma$ is about zero and equation (7) then predicts velocity weakening due to the intrinsic friction effect.

SUMMARY AND CONCLUSIONS

The data presented show that cyclic pure-shear loading of a simulated fault gouge results in net compaction and strain hardening for $\gamma < 0.5$-1.0, after which sliding occurs at roughly constant shear stress and net compaction ceases. Single-cycle loading produces less compaction than cyclic loading for a given shear strain. After the net compaction stage, dilatancy begins at about 25% of the peak stress for a given load cycle. The dilatancy rate $d\phi/d\gamma$ increases initially with strain, and $d^2\phi/d\gamma^2$ becomes negative at the peak stress, indicating that shear localization occurs at about the peak shear stress.

Experiments using Westerly granite samples with 60 to 320 grit surface roughnesses show a characteristic sudden drop in friction after 4-7 mm of slip, independent of gouge thickness. Identical experiments using a sample with grooved surfaces did not show the drop in friction. In addition, boundary shears are observed over one entire surface for experiments with 60-320 grit surfaces, whereas with the grooved-granite and steel samples, boundary shears are limited to half of each surface. This suggests that the drop in friction is associated with the formation of complete boundary shears.

Velocity stepping experiments indicate velocity strengthening (positive $a-b$) for shear within gouge and velocity weakening for slip between bare rock surfaces. The parameter $a-b$ varies inversely with normal stress and directly with gouge thickness and surface roughness. Our experiments with an initial gouge layer show corresponding changes in dilatancy rate and friction over step changes in load point velocity. Using an energy balance to relate changes in frictional resistance and dilatancy rate, we found quantitative agreement between the measured friction data and that predicted from changes in the dilatancy rate and a velocity weakening term. The magnitude of the change in friction calculated on the basis of changes in $d\phi/d\gamma$ decreases with decreasing gouge thickness, in agreement with the friction data.

Other work on gouge-rock friction indicates that shear localization may influence constitutive behavior and the stability of sliding [e.g., *Engelder et al.*, 1975; *Moore et al.*, 1988; *Tullis et al.*, 1989]. Our experiments show a progression from Riedel shears to fully developed boundary shears with increasing strain. Gouge sheared within rough surfaces shows only partially developed boundary shears, while smoother surfaces result in fully developed boundary shears. The difference in $a-b$ for grooved and 120 grit surfaces is on the order of the difference between 320 and 120 grit surfaces (which both contained boundary shears), and thus while boundary shears may cause $a-b$ to decrease, their development is not associated with a transition from velocity strengthening to velocity weakening.

We cannot rule out the possibility that further shear localization [e.g., *Mandl et al.*, 1977; *Tullis et al.*, 1989] will cause further reduction in $a-b$ and possibly velocity weakening. Indeed, *Tullis et al.* [1989] argue that this is the case. Our data show that for a granular gouge material, velocity strengthening occurs as a result of an increase in dilatancy rate upon an increase in slip rate. This provides an explanation for the common observation in laboratory experiments that the presence or accumulation of gouge tends to stabilize frictional sliding [e.g., *Scholz et al.*, 1972; *Byerlee and Summers*, 1976].

We cannot directly address the issue of whether velocity strengthening represents a long-term steady state behavior for natural fault gouge. In our experiments the gouge material reaches a roughly steady state particle-size distribution, which agrees with that obtained for a natural fault gouge [*Sammis et al.*, 1987]. However, the overall dilatancy that we observe must eventually give way to constant volume deformation or compaction. The situation along natural faults may be somewhat different. Unlike laboratory samples, which have ground surfaces and thus limited roughness, the roughness of natural faults is fractal [e.g., *Brown and Scholz*, 1985], and thus they undergo continual wear during displacement [*Scholz*, 1987; *Power et al.*, 1988]. The gouge zone within a natural fault therefore

continually incorporates new material, which is comminuted with further displacement. Faults with sufficiently high displacement (and/or wear) rates may therefore exhibit velocity strengthening if comminution and intense shear localization do not keep pace with the addition of new material. Indeed, as argued by *Marone and Scholz* [1988], a number of observations from faults with well-developed gouge zones and those within unconsolidated material indicate velocity strengthening at depths of less than 3-5 km. Our results may therefore be applicable to natural faults that have undergone significantly greater displacement than our experimental samples.

Acknowledgments. We thank Fred Chester, Keith Evans, and Ron Biegel for helpful discussions and thoughtful reviews of the manuscript. Terry Tullis, an anonymous reviewer, and Simon Cox are also thanked for reviews. Technical assistance by Ted Koczynski is gratefully acknowledged. Brian Evans and William Menke are thanked for reviews of an early version of the manuscript. Lamont-Doherty Geological Observatory contribution 4560.

REFERENCES

Biegel, R. L., C. G. Sammis, and J. H. Dieterich, The frictional properties of a simulated gouge with a fractal particle distribution, *J. Struct. Geol., 11*, 827-846, 1989.

Bishop, A. W., Discussion, *Geotechnique , 4*, 43-45, 1954.

Blanpied, M. L., T. E. Tullis, and J. D. Weeks., Frictional behavior of granite at low and high sliding velocity. *Geophy. Res. Lett., 14*, 554-557, 1987*a*.

Blanpied, M. L., T. E. Tullis, and J. D. Weeks, Contrasting velocity dependence of granite friction: initially bare surfaces vs. simulated gouge, *Eos Trans. AGU68*, 1478, 1987*b*.

Blanpied, M. L., T. E. Tullis, and J. D. Weeks, Textural and mechanical evolution of granite gouge in high-displacement sliding experiments. *Eos Trans. AGU 69*, 1463, 1988.

Brace, W. F., and J. D. Byerlee, Stick-slip as a mechanism for earthquakes, *Science, 153*, 990-992, 1966.

Brown, S. R., and C. H. Scholz, Broad bandwidth study of the topography of natural rock surfaces, *J. Geophys. Res., 90*, 12,575-12,582, 1985.

Byerlee, J. D., Frictional characteristics of granite under high confining pressure, *J. Geophys. Res., 72*, 3639-3648, 1967.

Byerlee, J., and R. Summers, A note on the effect of fault gouge thickness on fault stability, *Int. J. Rock Mech. Min. Sci. Geomech. Abstr., 13*, 35-36, 1976.

Byerlee, J., and P. Vaughan, Dependence of friction on slip velocity in water saturated granite with added gouge. *Eos Trans. AGU 65*, 1078, 1984.

Byerlee, J., V. Mjachkin, R. Summers, and O. Voevoda, Structures developed in fault gouge during stable sliding and stick-slip, *Tectonophysics, 44*, 161-171, 1978.

Chester, F. M., The brittle-ductile transition in a deformation-mechanism map for halite, *Tectonophysics, 154*, 125-136, 1988.

Conte, S. D., and C. de Boor, *Elementary Numerical Analysis: An Algorithmic Approach*, 432 pp., McGraw-Hill, New York, 1980.

Cox, S. J. D., Velocity dependent friction in a large direct shear experiment on gabbro, *Spec. Pub. Geol. Soc. London -Proceedings of Conference on Deformation Mechanisms, Rheology and Tectonics*, in press, 1990.

Crook, C. N., Geodetic measurements of horizontal crustal deformation associated with the October 15, 1979 Imperial Valley California earthquake, Ph. D. thesis, Univ. of London, 1984.

Dieterich, J. H., Modeling of rock friction: 1, Experimental results and constitutive equations. *J. Geophys. Res. 84*, 2161-2168, 1979.

Dieterich, J. H., Constitutive properties of faults with simulated gouge. in *Mechanical Behavior of Crustal Rocks, Geophys. Monogr. Ser. vol. 24*, edited by. N.L. Carter, M. Friedman, J. M. Logan, and D. W. Stearns, pp. 103-120, AGU Washington, D.C., 1981.

Dieterich, J. H., and G. Conrad, Effect of humidity on time- and velocity-dependent friction rocks, *J. Geophys. Res., 89*, 4196-4202, 1984.

Edmond, J. M., and M. S. Paterson, Volume changes during the deformation of rocks at high pressures. *Int. J. Rock Mech. Min. Sci. Geomech. Abstr., 9*, 161-182, 1972.

Engelder, J. T., Cataclasis and the generation of fault gouge, *Geol. Soc. Am. Bull., 85*, 1515-1522, 1974.

Engelder, J. T., J.M. Logan, and J. Handin, The sliding characteristics of sandstone on quartz fault-gouge, *Pure Appl. Geophys., 113*, 69-86, 1975.

Frank, F. C., On dilatancy in relation to seismic sources, *Rev. Geophys., 3*, 485-503, 1965.

Gu, J. C., J. R. Rice, A. L. Ruina, and S. T. Tse, Slip motion and stability of a single degree of freedom elastic system with rate and state dependent friction, *J. Mech. Phys. Solids, 32*, 167-196, 1984.

Healy, K. A., The dependence of dilation in sand on rate of shear strain, D. Sc. thesis, Mass. Inst. of Technol., Cambridge, 1963.

Hobbs, B. E., Chaotic behavior of frictional shear instabilities, paper presented at 2nd International Symposium on Rockburst in Mines, Univ. of Minn., 1988.

Johnson. T., Time dependent friction of granite: Implications for precursory slip on faults. *J. Geophys. Res., 86*, 6017-6028, 1981.

Lambe, T. W. and R. V. Whitman, *Soil Mechanics.*, New York, John Wiley, 1969.

Lockner, D. A., R. Summers, and J. D. Byerlee, Effects of temperature and sliding rate on frictional strength of granite, *Pure Appl. Geophys, 124*, 445-469, 1986.

Logan, J. M., M. Friedman, N. Higgs, C. Dengo, and T. Shimamoto, Experimental studies of simulated gouge and their application to studies of natural fault zones, Analyses of Actual Fault Zones in Bedrock, *U.S. Geol. Surv. Open File Rep., 79-1239*, 305-343, 1979.

Mandl, G., L. N. J. de Jong, and A. Maltha, Shear zones in granular material: an experimental study of their structure and mechanical genesis, *Rock Mech., 9*, 95-144, 1977.

Marone, C., Experimental studies of simulated fault gouge: frictional behavior, microstructures, and stability of sliding, Ph.D. thesis, 236 pp., Columbia Univ., New York, 1989.

Marone, C., and C. H. Scholz, The depth of seismic faulting and the upper transition from stable to unstable slip regimes, *Geophys. Res. Lett., 15*, 621-624, 1988.

Marone, C., and C. H. Scholz, Particle-size distribution and microstructures within simulated fault gouge. *J. Struct. Geol.,11*, 799-814, 1989.

Moore, D. E., R. Summers, and J. D. Byerlee, Relationship between textures and sliding motion of experimentally deformed fault gouge: Application to fault zone behavior, Key Questions in Rock Mechanics, edited by. P. A. Cundall, R. L. Sterling, and A. M. Starfield, Proc. 29th U.S. Symp. on Rock Mech., 103-110, 1988.

Morrow, C. A., D. Lockner, and J. D. Byerlee, Velocity- and time-dependent stress transients in simulated fault gouge, *Engineering in Complex Rock Formations*, International Society of Rock Mechanics, Beijing, 1986.

Muhlhaus, H. B., and I. Vardoulakis, The thickness of shear bands in granular materials, *Geotechnique, 37*, 271-283, 1987.

Power, W. L., T. E. Tullis, and J. D. Weeks, Roughness and wear during brittle faulting, *J. Geophys. Res.*, 93, 15,268-15,278, 1988.

Raleigh, C. B., and C. Marone, Dilatancy of quartz gouge in pure shear, *Mineral and Rock Deformation: Laboratory Studies, Geophys. Monogr. Ser., vol.* 36, edited by B.E. Hobbs, and H. C. Heard, pp. 1-10, AGU, Washinton, D.C., 1986.

Reynolds, O., On the dilatancy of media composed of rigid particles in contact, *Philos. Mag. Ser. 5, 20*, 469-481, 1885.

Rice, J. R., and A. L. Ruina, Stability of steady frictional slipping, *J. Appl. Mech., 50*, 343-349, 1983.

Rice, J. R., and J. Gu, Earthquake aftereffects and triggered seismic phenomena, *Pure Appl. Geophys., 121*, 187-219, 1983.

Roscoe, K. H., A. N. Schofield, and C. P. Wroth, On the yielding of soils, *Geotechnique, 8*, 22-53, 1958.

Ruina, A. L., Friction laws and instabilities: A quasistatic analysis of some dry frictional behavior, Ph.D. thesis, Brown Univ., 1980.

Ruina, A., Slip instability and state variable friction laws, *J. Geophys. Res., 88*, 10,359-10,370, 1983.

Sammis, C.G., G. King, and R. Biegel, The kinematics of gouge deformation, *Pure Appl. Geophys., 125*, 777-812, 1987.

Scholz, C. H., Wear and gouge formation in brittle faulting, *Geology, 15*, 493-495, 1987.

Scholz, C.H., M. Wyss, and S. W. Smith, Seismic and aseismic slip on the San Andreas fault. *J. Geophy. Res.*, *74*, 2049-2069, 1969.

Scholz, C.H., P. Molnar, and T. Johnson, Detailed studies of frictional sliding of granite and implications for the earthquake mechanism, *J. Geophys. Res.*, *77*, 6392-6406, 1972.

Shimamoto, T., and J. M. Logan, Effects of simulated fault gouge on the sliding behavior of Tennessee sandstone: nonclay gouges, *J. Geophys. Res.*, *86*, 2902-2914, 1981.

Shimamoto, T., and J. M. Logan, Velocity-dependent behavior of simulated halite shear zones: An analog for silicates, *Earthquake Source Mechanics, Geophys. Monogr. Ser.*, vol. 37, edited by S. Das, J. Boatwright, and C. H. Scholz, pp. 49-63, AGU, Washington, D.C., 1986.

Solberg, P., and J. Byerlee, A note on the rate sensitivity of frictional sliding of Westerly granite, *J. Geophys. Res.*, *89*, 4203-4205, 1984.

Stuart, W. D, Strain softening prior to two-dimensional strike-slip earthquakes, *J. Geophys. Res.*, *84*, 1063-1070, 1979.

Tullis, T. E., Rock friction constitutive behavior from laboratory experiments and its implications for an earthquake prediction field monitoring program, *Pure Appl. Geophys.*, *126*, 555-588, 1988.

Tullis, T. E., and J. D. Weeks, Constitutive behavior and stability of frictional sliding of granite, *Pure Appl. Geophys.*, *124*, 383-414, 1986.

Tullis, T. E., M. L. Blanpied, and J. D. Weeks, The velocity dependence of granite friction with and without simulated gouge, *Eos Trans. AGU*, *70*, 1302, 1989.

Weeks, J. D., and T. E. Tullis, Frictional behavior of dolomite: a variation in constitutive behavior, *J. Geophys. Res.*, *90*, 7821-7826, 1985.

Williams, P. L., and H. W. Magistrale, Slip along the Superstition Hills faults associated with the 24 November 1987 Superstition Hills, California, earthquake, *Bull. Seismol. Soc. Am.*, *79*, 390-410, 1989.

C. Marone, Department of Geology, University of Melbourne, Parkville, Victoria, 3052 Australia.

C. B. Raleigh, School of Ocean, Earth Science and Technology, University of Hawaii, Honolulu, HI 96822.

C. H. Scholz, Lamont-Doherty Geological Observatory, Palisades, NY 10964.

(Received March 15, 1989;
revised August 14, 1989;
accepted August 30, 1989.)